universität wien

MASTERARBEIT / MASTER'S THESIS

Titel der Masterarbeit / Title of the Master's Thesis

„Investigating a Molybdenum Complex using a Density Matrix Renormalization Group Method“

verfasst von / submitted by

Leopold Lindenbauer BSc

angestrebter akademischer Grad / in partial fulfilment of the requirements for the degree of

Master of Science (MSc)

Wien, 2023 / Vienna, 2023

Studienkennzahl lt. Studienblatt / degree programme code as it appears on the student record sheet:	A 066 862
Studienrichtung lt. Studienblatt / degree programme as it appears on the student record sheet:	Masterstudium Chemie
Betreut von / Supervisor:	Univ.-Prof. Dr. Dr. h.c. Leticia González

ABSTRACT

A novel quantum chemical method was used to calculate the properties of a compound with possible application in photodynamic therapy. The organometallic complex dicarbonyl(η^5-2,4-cyclopentadien-1-yl)-nitrosyl-molybdenum, $CpMo(CO)_2NO$, features the two biologically active groups NO and CO. Excited electronic states are calculated and analyzed to investigate selective dissociation of these groups.

The transition metal core, a nitrosyl group, and conjugated π-systems make this compound challenging for quantum-chemical methods. In a wavefunction-based approach, these challenges may be met with multi-reference methods, but computational demands limit the size and complexity of analyzable systems. The novel Density Matrix Renormalisation Group (DMRG) method is explored as a tool to reduce the computational effort by automatically identifying and discarding confgurations with negligible influence.

Density Functional Theory (DFT) was used to calculate an equilibrium geometry for the compound. This molecular geometry was then analyzed using DMRG and DFT. The results were compared to available experimental IR-spectroscopy and crystallography data, and the predictions for the UV-Vis spectrum of the compound were discussed. The electronic transitionis were analyzed for their Charge-Transfer character, and possible candidate states for selective dissociation were identified.

The DMRG orbital selection protocol was modified to improve the representation of excited states that might become important during the dissociation.

Using DMRG, the dissociation of the CO ligand was analyzed by calculating the electronic properties of the system at increasing elogations of one of the Me−CO bonds.

Using DFT, the dissociation of both the NO and CO ligands was analyzed by separate calculations of the resulting fragments. These calculations were then used to predict the dissociation energies for the NO and CO ligands.

ZUSAMMENFASSUNG

Eine neuartige quantenchemische Methode wurde verwendet, um ein Molekül auf dessen Anwendbarkeit für photodynamische Therapie zu untersuchen. Der Organometallkomplex dicarbonyl-(η^5-2,4-cyclopentadien-1-yl)-nitrosyl-Molybdän ($CpMo(CO)_2(NO)$) enthält eine Nitrosyl- und zwei Carbonyl-Gruppen als Liganden, die eine direkte therapeutische Wirkung entfalten können. Angeregte Zustände wurden analysiert, um die selektive Dissoziation dieser beiden Liganden zu untersuchen.

Das Übergangsmetall-Zentrum, die konjugierten π-Systeme und die Nitrosyl-Gruppe stellen für quantenchemische Berechnungsmethoden eine Herausforderung dar. Methoden, die auf der Elektronen-Wellenfunktion beruhen, begegnen diesen Herausforderungen, indem sie angeregte elektronische Zustände in die Berechnung mit einbeziehen, wobei der steigende Berechnungsaufwand hier Grenzen setzt. Hier wurde die neuartige Density-Matrix-Renormalisation-Group-Methode (DMRG) wurde verwendet, die Zustände mit gerigem Beitrag während der Berechnung identifizieren und ausklammern kann.

Die Grundzustands-Geometrie wurde mit Dichtefunktional-Theorie (DFT) als Ausgangspunkt berechnet und mit früheren Arbeiten zu diesem Komplex verglichen. Diese Geometrie wurde mit DMRG und DFT weiter analysiert und die Ergebnisse mit experimentellen IR-spektroskopischen und Röntgen-kristallographischen Daten verglichen. Aus den berechneten Elektronendichten wurden die Übergangsdichten für elektronische Anregungen auf deren Charge-Transfer-Charakter untersucht, um Kandidaten für dissoziative Übergänge zu identifizieren.

Das DMRG-Auswahlverfahren für die Orbitale wurde angepasst um angeregte Zustände besser zu berücksichtigen, die während der Dissoziation relevant werden können.

Mit DMRG wurde die Dissoziation von CO mit der DMRG-Methode analysiert, indem die Länge der $Mo-CO$-Bindung in mehreren Schritten erhöht und die elektronischen Eigenschaften berechnet wurde. Mit DFT wurden die CO- und NO-Gruppen direkt von der Grundzustands-Geometrie abgetrennt und die Fragmente einzeln analysiert. Auf diese Weise wurden Vorhersagen für die Dissoziationsenergie der NO- und CO-Liganden getroffen.

ACKNOWLEDGMENTS

I would like to thank Prof. Leticia González for giving me the opportunity to join the González Research Group and explore the world of quantum chemistry. This thesis was made possible by the guidance, aid, and encouragement I received from the members of this group and I would like to thank them all. Dr. Markus Oppel and Dr. Leon Freitag provided me with the essential scientific support to move the project forward. My office-mates Dr. Moritz Heindl and Dr. Davide Avagliano guided me with profound answers to my confused questions about life, the universe, and everything. Fellow candidates Nadia, Omar, Anna, and Ludwig shared in our challenges, solutions, and successes. I want to thank everyone in the group for making me feel welcome and providing an environment full of scientific and personal growth.

I am equally thankful for my friends and family who patiently shared their counsel, help, and excitement in the progress of the present work. This journey would hot have been possible without them.

DEDICATION

For some reason, the *billiard ball* has come to play the role of the prototype of a classical particle in textbooks on quantum mechanics. The author, of course, conforms to this tradition.

It may amuse the reader to know that the author has never played billiards and has never held a billiard ball in his hand. His knowledge of the alledged properties of billiard balls is, therefore, book knowledge, derived from texts on quantum mechanics.

— Eyvind Wichmann, Berkeley Physics Course - Quantum Physics

LIST OF SYMBOLS

Symbol	Description
$\mathbf{r}$	Generic spatial coordinates, Electronic spatial coordinates
$\mathbf{R}$	Nuclear spatial coordinates
$\mathbf{x}$	Electronic spatial coordinates with spin coordinate
τ	Integration variable
t	Time
$\hbar$	Planck's constant
i	Imaginary unit
E	Energy
$\{\ \}$	Set
N	Set cardinality
r_{ij}	Distance between two bodies
$\mathbf{A}$	Matrix A
A_{ij}	Element ij of matrix A
$_N$	Specifier for nuclear context
$_e$	Specifier for electronic context
$_{A,\,B}$	Indices for nuclei
$_{i,\,j}$	Indices for electrons
$_{\mu,\,\nu}$	Generic indices
$\hat{O}$	Operator O
$\hat{H}$	Hamilton operator
$\hat{T}$	Kinetic energy operator
$\hat{V}$	Potential energy operator
∇	Nabla operator
$\hat{P}$	Permutation operator
$F[f]$	Functional F of function f
ψ	Generic wave function
$\lvert\psi\rangle$	Generic wave function in Dirac notation
ϕ^*	Complex conjugate of wave function ϕ
$\langle\phi\rvert$	Complex conjugate of wave function ϕ in Dirac notation
χ	Spin orbital
Ψ	Generic Slater determinant
Ψ_i	Excited Slater determinant
δ_{ij}	Kronecker delta

Symbol	Description
ρ	Electron density
$f(p;x)$, $f(\overline{p})$	Function f is parametrically dependent on p
Z	Nuclear charge
$\angle(A-B-C)$	Aangle at atom B between atoms A and C
$s(1)_i$	Single-orbital entropy of orbital i
$s(2)_{ij}$	Two-orbital entropy of orbitals i and j
$s(n)_{A,S}$	n-orbital entropy of orbital(s) A in electronic state S
I_{ij}	Mutual Information between orbitals i and j
$\max_S x_S$	The largest value of x_S, considering all values of the index S

1 INTRODUCTION

1.1 PHOTODYNAMIC THERAPY

Photodynamic Therapy (PDT) is a clinically approved, minimally invasive therapeutic procedure. Its mechanism is the generation of cytotoxic molecular species inside the targeted cells - typically cancer cells - to disrupt their metabolism and kill them. The species are generated by the action of visible or near-visible light on a photosensitizer. The mechanism of action is classified by the nature of the cytotoxic species: If an excited state of the photosensitizer itself is cytotoxic, the mechanism is classified as Type I. If the excited photosensitizer transfers the energy to molecular oxygen, exciting it from the triplet ground state ($^3O_2$) to the singlet ground state ($^1O_2$), the mechanism is classified as Type II. Singlet oxygen is exceptionally reactive and short-lived in a biological medium, and has been shown to be toxic to essentially every component of a cell [1].

The technique has several advantages over other, established anti-cancer therapies that make it an attractive goal for research. It is non-invasive for dermal application and minimally invasive when using endoscopes. In contrast to chemotherapy, the drug component is inactive in the absence of light and may be entirely harmless to the body [2]. In contrast to both radio- and chemotherapy, the radiation used in PDT does not confer the risk of immunosuppression. The local inflammatory response due to the tumor cell damage is believed to increase the antitumor activity of the immune system. A challenge to the method is the hypoxic, oxygen-depleted environment of tumor cells, reducing the effectiveness of the Type II mechanism. Research on PDT with chemical scope is focused on the development and improvement of photosensitziers by tuning the activation wavelength or enabling the sensitizers to target specific cells and organelles within them, so that the generated singlet oxygen is used more efficiently [1].

The use of an alternative mechanism has been proposed, where the photosensitive molecule undergoes dissociation and releases a therapeutically active fragment. Of particular interest is the use of organometallic complexes that release CO or NO after photoactivation [3][4]. Both CO and NO have a wide variety of physiological functions and effects, both being linked to inflammatory response and blood pressure regulation [5][6]. The photo-regulated activity of these effects could then extend the capabilities of PDT beyond the scope of cytotoxic mechanisms.

This thesis will examine a molybdenum complex containing both CO and NO, with the goal of finding conditions where it is possible to selectively dissociate either one of these fragments. This would enable to tune the therapeutic effects of a single administered drug by switching on and off specific light sources.

1.2 MOLYBDENUM COMPLEX

The target molecule for this study is dicarbonyl(η^5-2,4-cyclopentadien-1-yl)nitrosyl-molybdenum, $CpMo(CO)_2NO$, where Cp is the cyclopentadienyl-anion $C_5H_5^-$. This molecule has already been considered as a possible NO-releasing agent for use in humans, to act as a vasodilation drug. Closely related transition metal nitrosyls have been used in *in vivo* animal tests and a number of synthetic routes are available [7].

The Mo metal center is a necessary trace element in human diet. It is a component of the cofactor molybdopterin and is coordinated to the FeS-cluster of nitrogenase in some bacteria [8]. As such, it is ubiquitous in food and no dietary plans are known to cause a deficiency [9]. Leichtmann and Sitrin [10](as cited in [9]) estimate a daily intake via food of 150 µg - 500 µg to be adequate for humans. The main factor in the toxicity of Mo is the well-established interaction with the metabolism of copper. Molybdenum intake can be toxic when copper uptake is insufficient, leading to weight loss and anemia in animal trials, which were reversible by increase of dietary copper uptake. Organs that accumulate Mo (e.g. liver, kidneys, bones, adrenals and omentum) may be damaged by higher exposure. If the exposure is removed, excess Mo is then quickly eliminated from the body by urinary excretion [9], where the expected absolute Mo content is in the range of 9 mg for a hypothetical average human male weighing 70 kg [11]. Therefore, the use of Mo in a drug, especially in treating severe diseases, seems to offer opportunities within acceptable risks.

1.3 AB-INITIO INVESTIGATION

This thesis attempts an *ab initio* analysis of the Mo-complex. Density Functional Theory (DTF) is a widely used method for investigating transition metal complexes [12]. The NO-ligand, however, requires a cautious approach due to its *non-innocence*. The concept was proposed by Jørgensen [13] (as cited in [14]) to denote ligands whose oxidation state is not *a priori* obvious[14]. The charge on NO impacts its ligand behaviour, as electron-rich NO may be attached at an angle, while neutral and positively charged NO tends to be linearly attached [15].

It is thus expected that the non-innocence of the NO-ligand, the dissociation of the molecule, and the π-bonds in the ligands introduce a large amount of static correlation between the electrons of the system.

The proper description of this static correlation requires methods that include multiple electronic configurations [16].

The Density Matrix Renormalization Group (DMRG) method in its quantum chemical formulation [17] [18] [19] [20] [21] [22] is able to recover this static correlation and has been used successfully in the analysis of similar complexes [16]. This thesis will investigate the applicability of the DMRG method to the analysis of the photo-induced dissociation of the Mo-complex.

The investigation will be presented in the remainder of this thesis. The theoretical background is presented in section 2. The methods, implementations, and procedures are described in section 3. The results are presented and discussed in section 4, subdivided thematically into the treatments of the equilibrium geometry in section 4.1, the excited states in section 4.2, and ligand dissociation in section 4.3. Section 5 concludes the investigation by providing a summary of the findings. The appendix contains tabular data and selected illustrations of the molecular orbitals generated during the investigation.

Results and findings obtained during the creation of this thesis have been published as Freitag et al. [23].

2 THEORY

This chapter gives an overview of the methods and approximations used to analyze the molybdenum complex. Describing the chemical behavior of a molecule is at the very core a question of the behavior of the electrons in response to movement of the atomic cores and external potentials. Electronic Structure Theory is the theoretical framework which encompasses the methods used to describe electrons that are bound to atoms.

2.1 THE SCHRÖDINGER EQUATION

The quantum mechanical theory introduced by Schrödinger [24][25] posits that all observable features of a physical system can be calculated from a function $\psi(\mathbf{r}, t)$ in terms of the position $\mathbf{r}$ of the particles constituting the system, and time t. ψ is called the wave function of the system. The wave function is generated by solving the central equation of quantum mechanics, the time-dependent Schrödinger equation

$$\hat{H}\psi(\mathbf{r}, t) = i\hbar\frac{\partial}{\partial t}\psi(\mathbf{r}, t), \tag{2.1.1}$$

where the Hamilton operator $\hat{H}$ contains all interactions within the system under consideration and for a general N-particle-system is

$$\hat{H}(\mathbf{r}, t) = \hat{T}(\mathbf{r}) + \hat{V}(\mathbf{r}, t), \tag{2.1.2}$$

where $\hat{T}(\mathbf{r})$ and $\hat{V}(\mathbf{r}, t)$ are the operators for the kinetic and potential energy of the particles.

For systems in a bound state where $\hat{V}$ and thus by extension $\hat{H}$ are time-independent, the energy E of the system is constant. E is then an eigenvalue of $\hat{H}$ with respect to $\psi(\mathbf{r}, t)$, so that $\psi(\mathbf{r}, t)$ can also be separated into a time-dependent and space-dependent part [26]

$$\begin{aligned} \hat{H}(\mathbf{r})\psi(\mathbf{r}, t) = E\psi(\mathbf{r}, t) &= i\frac{\partial}{\partial t}\psi(\mathbf{r}, t) \\ \psi(\mathbf{r}, t) &= \psi(\mathbf{r})e^{-iEt}. \end{aligned} \tag{2.1.3}$$

The spatial wave function is multiplied by a simple phase factor. For time-independent systems, this phase factor can typically be neglected.This leads to a compact notation for the time-independent Schrödinger equation

$$\hat{H}\psi(r) = E\psi(r). \tag{2.1.4}$$

This form of the Schrödinger equation will be used for the rest of this thesis.

2.1.1 *Wave Functions*

Acceptable wave functions that are solutions to the time-independent Schrödinger equation are complex-valued and depend on the coordinates of all particles, $\psi(\mathbf{r})$. The interpretation of the physical meaning of these functions is subject to debate, but the square of its absolute value $|\psi(\mathbf{r}, t)|^2$ is generally accepted to be proportional to the probability density of finding the particles at positions $\mathbf{r}$. To allow for this interpretation, the wave function must be square-integrable and yield a normalized probability density such that

$$\int_{-\infty}^{\infty} |\psi(\mathbf{r})|^2 d\mathbf{r} = 1. \tag{2.1.5}$$

As the operators used with the Schrödinger equation typically include differential operators, the wave function is required to be continuous and differentiable on the domain of the function.

For the molecules investigated in this thesis, the coordinates of the electrons are given as $\mathbf{r}$ and the coordinates of the nuclei are given as $\mathbf{R}$.

2.1.2 *Dirac Notation*

Throughout this thesis, the Dirac notation [27] will be used, where the symbol $|\psi\rangle$ denotes a wave function with the label ψ that may be inserted into a given quantum mechanical formalism. The wave function may be given either as an n-dimensional vector or as a function of spatio-temporal coordinates. This ambiguity is more than compensated by the ease of use that comes with it, as the vector and function representation are equivalent and may be converted from one to the other as needed. The complementary symbol $\langle\psi|$ is then the complex conjugate of $|\psi\rangle$, and additionally its transposed form when it is a vector. Combining both symbols in the form of $\langle\psi \,|\, \phi\rangle$ gives the inner product. When ϕ and ψ are given in the form of functions, the inner product is defined as the integral

$$\int_a^b \psi^*(x)\phi(x)\, dx, \tag{2.1.6}$$

where the ϕ^* denotes the complex conjugate of ϕ, x denotes all coordinates of the system, and a and b are the boundaries of the system under consideration. When treating molecular systems, the whole space is considered, with the borders set at positive and negative infinity. The function resulting from the action of an operator $\hat{O}$ on a wave function is denoted as $\hat{O}\,|\psi\rangle$. A common occurrence is to take the inner product of such a function, such as $\langle\psi \,|\, \hat{O} \,|\, \psi\rangle$, where it will denote the operator acting on the function to the right. In the vector formalism, it is simple to construct operators that act to the left,

which are the adjoint of the matrix of the corresponding right-acting operator.

The equivalence of the vector and function formalisms can be shown by decomposing the function ψ as a sum of suitable basis functions ψ_i as $\psi = \sum c_i \psi_i$. The coefficients c_i are then assigned as the elements of the vector representation of the function ψ. If the basis functions are orthonormal to each other, i. e. , $\langle \phi_i | \phi_j \rangle = \delta_{ij}$, where δ_{ij} is the Kronecker delta with

$$\delta_{ij} = \begin{cases} 1, & \text{if } i = j, \\ 0, & \text{if } i \neq j. \end{cases} \tag{2.1.7}$$

It can be shown that the effect of an operator $\hat{O}\psi = \psi'$ can be represented as the action of the operator on the individual basis functions, so that $\psi' = \sum_j c'_j \phi_j = \sum_j \sum_i \hat{O} c_i \phi_i = \sum_{ij} O_{ij} c_i \phi_i$, where O_{ij} is then the matrix representation of the operator $\hat{O}$.

If the wave function is an eigenfunction of the operator, the eigenvalues are evaluated by taking the inner product of the eigenvalue equation with the complex conjugate of the wave function

$$\begin{aligned} \hat{O} |\psi\rangle &= O |\psi\rangle \\ \langle \psi | \hat{O} | \psi \rangle &= O \langle \psi | \psi \rangle \\ \frac{\langle \psi | \hat{O} | \psi \rangle}{\langle \psi | \psi \rangle} &= O, \end{aligned} \tag{2.1.8}$$

with O being the eigenvalue associated with the operator $\hat{O}$.

2.1.3 *The Hamilton Operator*

The Hamilton operator receives its name from its similarity to the Hamilton formulation of classical mechanics. It is the sum of the kinetic and potential energy terms, which, in quantum mechanics, reads as:

$$\hat{H} = \hat{T} + \hat{V}. \tag{2.1.9}$$

The kinetic energy operator $\hat{T}$ is given as

$$\hat{T} = -\frac{\hbar^2}{2m} \nabla^2, \tag{2.1.10}$$

where ∇ is called the nabla operator and represents a differentiation in all spatial coordinates. $\hbar$ is the reduced Planck's constant $\hbar = \frac{h}{2\pi}$. In Cartesian coordinates, this resolves to

$$\nabla_i^2 = \left[\frac{\partial^2}{\partial x_i^2} + \frac{\partial^2}{\partial y_i^2} + \frac{\partial^2}{\partial z_i^2} \right] \tag{2.1.11}$$

for each particle i under consideration.

The time-independent potential energy operator $\hat{V}$ is constructed as the sum of all coulomb interactions between the particles of the

system, depending on their positions. When given in atomic units with the electron mass m_e, the elementary charge e, the reduced Planck constant $\hbar$, and the prefactor of Coulomb's law $\frac{1}{4\pi\epsilon_0}$ all equal to unity, the Hamiltonian operator for a molecule can be written as

$$\begin{aligned}
\hat{H} &= \hat{T}_e + \hat{T}_N + \hat{V}_{ee} + \hat{V}_{Ne} + \hat{V}_{NN} \\
\hat{T}_e &= -\sum_i \frac{1}{2}\nabla_i^2 \\
\hat{T}_N &= -\sum_A \frac{1}{2M_A}\nabla_A \\
\hat{V}_{ee} &= \sum_i \sum_{j>i} \frac{1}{|\mathbf{r}_i - \mathbf{r}_j|} \\
\hat{V}_{Ne} &= -\sum_A \sum_i \frac{Z_A}{|\mathbf{R}_A - \mathbf{r}_j|} \\
\hat{V}_{NN} &= \sum_A \sum_{B>A} \frac{Z_A Z_B}{|\mathbf{R}_A - \mathbf{R}_B|}.
\end{aligned} \tag{2.1.12}$$

As with most other operators, the Hamiltonian may have more than one eigenfunction. The eigenfunction giving the lowest energy represents the ground state[1], the other wave functions then represent excited states.

2.1.4 *Born-Oppenheimer-Approximation*

Born and Oppenheimer [28] showed that it is a valid approximation to treat the movement of the nuclei of a molecule separately from the electrons. The mass of an electron is smaller than that of a proton by three orders of magnitude. Under this approximation, the electrons are able to instantaneously follow movements of the atomic cores. So, when treating the nuclei as stationary point charges, the total electronic energy E_{elec} of a molecule is then recovered by the electronic Schrödinger equation

$$\hat{H}_{elec} \left|\psi_{elec}\right\rangle = E_{elec} \left|\psi_{elec}\right\rangle, \tag{2.1.13}$$

with the electronic Hamiltonian $\hat{H}_{elec} = \hat{T}_e + \hat{V}_{ee} + \hat{V}_{Ne} + \hat{V}_{NN}$. The operators $\hat{V}_{Ne}$ and $\hat{V}_{NN}$ depend on the given geometry of the nuclei, so the wave function $|\psi_{elec}\rangle$ also depends on the nuclear geometry. For each nuclear geometry, the electronic Schrödinger equation needs to be solved independently. This is expressed as ψ_{elec} and E_{elec} being *parametrically dependent* on the nuclear coordinates $\mathbf{R}$, and denoted by the symbols $\psi_{elec}(\mathbf{R};\mathbf{r})$ and $E_{elec}(\overline{\mathbf{R}})$, with $\mathbf{r}$ denoting the electronic coordinates.

The movement of the atomic cores can then be treated in a quantum mechanical way by creating a potential energy surface (PES). This

1 it is possible that multiple wave functions give identical energy values, making the states degenerate.

yields the electronic energies $E_{elec}(\overline{\mathbf{R}})$ as a function of the nuclear coordinates $\mathbf{R}$.

2.1.5 *Variational Principle*

The variational principle ensures that any wave function that solves the Schrödinger equation gives a value for the energy of the system that is an upper bound to the energy of the exact solution. A given trial function Φ_i could be considered as an expansion $\Phi_i = \sum_i a_i \psi_i$ of all exact solutions ψ_i to $\hat{H} |\psi\rangle_i = E_i |\psi\rangle_i$, ordered in i by increasing energy with E_0 being the ground state energy. [26] The energy W for the trial function is then

$$\begin{aligned} W &= \frac{\langle \Phi | \hat{H} | \Phi \rangle}{\langle \Phi | \Phi \rangle} \\ W &= \frac{\sum_{ij} a_i a_j \langle \Phi_i | \hat{H} | \Phi_j \rangle}{\sum_{ij} a_i a_j \langle \Phi_i | \Phi_j \rangle} \\ W &= \frac{\sum_i a_i^2 E_i}{\sum_i a_i^2} \\ W - E_0 &= \frac{\sum_i a_i^2 E_i}{\sum_i a_i^2} - E_0 \\ W - E_0 &= \frac{\sum_i a_i^2 (E_i - E_0)}{\sum_i a_i^2}, \end{aligned} \tag{2.1.14}$$

where the orthogonality of the ψ_i is used. Both a_i^2 and $(E_i - E_0)$ are non-negative by their definition, so this is also true for $W - E_0$. The equality $W = E_0$ only holds true if the trial wave function is the ground state wave function, or is a linear combination of degenerate ground state wave functions.

When trying to compute the energy of a molecule, it is not feasible to search the complete set of all valid wave functions. The variational principle makes it possible to select a certain subset of wave functions and compute the minimal energy that can be achieved within this subset. The subset can then be chosen such that the search for the minimum energy is efficient and can be finished with reasonable computational effort.

2.2 HARTREE-FOCK METHOD

Finding exact analytical solutions for the electronic Schrödinger equation 2.1.13 with a molecular Hamiltonian is not possible for molecules consisting of more than one electron. The Hartree-Fock method treats each electron as moving within the average field generated by the other electrons in the molecule [29][30]. This approximation is also termed *mean-field theory*. The method then tries to solve the Schrödinger equation iteratively by compiling a set of orbitals occupied by the electrons,

calculating the generated field, and using this field to generate a new set of orbitals. If the fields generated in two consecutive steps are similar enough, i. e. , the mean field produces orbitals that in turn produce the same field, the calculation is considered as completed. This solution is called a *self-consistent field* (SCF).

2.2.1 *Slater Determinants*

The wave function used in the Hartree-Fock method has to satisfy the Pauli principle for fermions, which demands that a given electronic wave function must be anti-symmetric under exchange of two electrons and, in direct consequence, be zero if two or more electrons with identical spin occupy the same orbital. To treat the fermionic character of the electrons, the spin coordinate ω is included in the electronic coordinates, which are then denoted as $\mathbf{x}$. The spin orbitals $\chi_n(\mathbf{x})$ are composed from spatial orbitals $\psi_i(\mathbf{r})$ multiplied by one of the spin functions $\alpha(\omega)$ or $\beta(\omega)$ in the spin coordinate ω. Constructing a wave function for N electrons as a Hartree product

$$\psi^{HP} = \prod_i \chi_i(\mathbf{x}_i) \tag{2.2.1}$$

of spin orbitals χ_i does not satisfy the Pauli principle, but it is possible to combine multiple Hartree products to give a wave function with the desired property.

The construction scheme and resulting wave function is called Slater determinant [31], and is defined as

$$|\Psi(\mathbf{x}_1, \mathbf{x}_2, ..., \mathbf{x}_N)\rangle = \frac{1}{\sqrt{N!}} \begin{vmatrix} \chi_1(\mathbf{x}_1) & \chi_2(\mathbf{x}_1) & \cdots & \chi_N(\mathbf{x}_1) \\ \chi_1(\mathbf{x}_2) & \chi_2(\mathbf{x}_2) & \cdots & \chi_N(\mathbf{x}_2) \\ \vdots & \vdots & & \vdots \\ \chi_1(\mathbf{x}_N) & \chi_2(\mathbf{x}_N) & \cdots & \chi_N(\mathbf{x}_N) \end{vmatrix} . \tag{2.2.2}$$

A shorthand notation will be used, where only the indices of one of the elements (spin orbitals or fermion coordinates) are given. The other indices are understood to be in linear order, and the normalization constant $\frac{1}{\sqrt{N!}}$ is implied by giving N itself [32]. The determinant given above is then written as

$$|\Psi(\mathbf{x}_1, \mathbf{x}_2, ..., \mathbf{x}_N)\rangle \equiv |12...N\rangle . \tag{2.2.3}$$

2.2.2 *Fock Operator*

The mean-field approximation is formulated as the Hartree-Fock equation

$$\hat{f} |\chi_a\rangle = \epsilon_a |\chi_a\rangle , \tag{2.2.4}$$

where the χ_i are the spin orbitals of the electrons, ϵ_i are the corresponding orbital energies and $\hat{f}$ is the Fock operator [32]. The Fock operator $\hat{f}(i)$ for electron i is given as

$$\hat{f}(i) = \hat{h}(i) + \hat{v}^{HF}(i) \tag{2.2.5}$$

with the one-electron operator $\hat{h}(i)$ for the kinetic energy of the electron and the Coulomb interaction with the nuclei as

$$\hat{h}(i) = -\frac{1}{2}\nabla_i^2 - \sum_A \frac{Z_A}{r_{iA}}, \tag{2.2.6}$$

and the operator for the Hartree-Fock potential $v^{HF}(1)$, an effective one-electron potential resulting from the other electrons in the system with

$$\begin{aligned} \hat{v}^{HF}(i) &= \sum_b \left(\hat{\mathcal{J}}_b(i) - \hat{\mathcal{K}}_b(i)\right) \\ \hat{\mathcal{J}}_b(i)\chi_a(i) &= \left[\int d\mathbf{x_j}\, \chi_b^*(j)\frac{1}{r_{ij}}\chi_b(j)\right]\chi_a(i) \\ \hat{\mathcal{K}}_b(i)\chi_a(i) &= \left[\int d\mathbf{x_j}\, \chi_b^*(j)\frac{1}{r_{ij}}\chi_a(j)\right]\chi_b(i), \end{aligned} \tag{2.2.7}$$

where $\hat{\mathcal{J}}_b(i)\chi_a(i)$ represents the action of the coulomb repulsion between two electrons when electron i occupies spin orbital χ_a and electron j occupies orbital χ_b, and $\hat{\mathcal{K}}_b(i)\chi_a(i)$ represents the potential arising from the exchange of the two electrons and has no classical interpretation. While the mean-field theory formally excludes the interaction of an electron with itself, the Coulomb and exchange potential for such a self-interaction cancel each other out as

$$\left[\hat{\mathcal{J}}_a(i) - \hat{\mathcal{K}}_a(i)\right]\chi_a(i) = 0. \tag{2.2.8}$$

which permits their inclusion in the sum over all electron-electron interactions, simplifying the algebra. It is desirable to write the action of $\hat{\mathcal{K}}_b(i)$ in such a way that the indices of the orbitals line up with the indices of the integral. A permutation operator $\hat{\mathcal{P}}_{12}$ can be introduced that swaps the indices of electron i and electron j, so that the action of $\hat{\mathcal{K}}$ can be written as

$$\hat{\mathcal{K}}_b(i)\chi_a(i) = \left[\int d\mathbf{x_j}\, \chi_b^*(j)\frac{1}{r_{ij}}\hat{\mathcal{P}}_{12}\chi_b(j)\right]\chi_a(i) \tag{2.2.9}$$

and all terms of $\hat{f}$ reduce to the compact form of equation 2.2.4 given above, presented as an eigenvalue equation. However, the integrals contained in $\hat{\mathcal{J}}$ and $\hat{\mathcal{K}}$ represent the effects of the mean-field, dependent in turn on $|\chi_a\rangle$. This nonlinear dependence is treated by solving the eigenvalue equation iteratively, using integrals of a previous iteration step to generate a new $|\chi_a\rangle$.

2.2.3 *Basis Sets*

When the spatial orbitals ψ_i used in the Slater determinant are expanded in terms of a basis set $\{\phi_\mu\}$ as

$$\psi_i = \sum_\mu C_{\mu i}\phi_\mu, \tag{2.2.10}$$

the Hartree-Fock-Equations become

$$\hat{f}(1)\sum_\nu C_{\nu i}\phi_\nu(1) = \epsilon_i \sum_\nu C_{\nu i}\phi_\nu(1) \tag{2.2.11}$$

and can be transformed into a matrix equation by multiplying with ϕ_ν^* from the left and integrating over the whole space [32]:

$$\sum_\nu C_{\nu i}F_{\mu\nu} = \epsilon_i \sum_\nu C_{\nu i}S_{\mu\nu} \tag{2.2.12}$$

with the Fock matrix $F_{\mu\nu} = \int d\mathbf{r}_1\, \phi_\mu^*(1)\hat{f}(1)\phi_\mu(1)$ and the overlap matrix $S_{\mu\nu} = \int d\mathbf{r}_1\, \phi_\mu^*(1)\phi_\mu(1)$. This gives the Roothaan [33] matrix equation

$$\mathbf{FC} = \mathbf{SC}\boldsymbol{\epsilon} \tag{2.2.13}$$

which can be solved efficiently by modern computers.

The choice of the basis set $\{\phi_\mu\}$ determines the accuracy of the Hartree-Fock method. As the variational principle holds for solutions obtained by this method, adding more basis functions increases the function space available to approach the exact solution. This is a strategy to improve the final energy. However, this also increases the computational effort, and the main contribution is the calculation of integrals for the interaction of two electrons. The number of these integrals increases as $\frac{1}{8}L^4$ [32], where L is the cardinality of the basis set. This gives a computational complexity of $\mathcal{O}(L^4)$ for the method, which dominates the contribution from solving the matrix eigenvalue equation, which scales as $\mathcal{O}(L^3)$.

While basis sets composed of radial Slater functions more closely model the exponential radial decay of the exact wave function of the hydrogen atom and the cusp at the nucleus, these functions lead to integrals that have to be approximated [34] or solved numerically [35]. When using Gaussian basis functions, the relevant integrals have known exact solutions [36][37], which allows fast and efficient evaluation [38].

2.2.4 *Electron Correlation*

In the Hartree-Fock method, the electron-electron interaction is treated in an average way, which is also reflected by using a wave function for uncorrelated particles. This approximation is sufficient to allow for a qualitative description of the system, but cannot describe systems

where the correlated movement of the electrons is an important factor. This electron correlation can be divided into dynamical and non-dynamical contributions, with dynamical contributions coming from the instantaneous movement of electrons, e. g. those occupying the same spatial orbital, and non-dynamical contributions from electrons occupying different spatial orbitals with near-degenerate energy levels [26].

The correlation energy E_{corr} is given as the difference between the exact solution of the non-relativistic Schrödinger equation and the Hartree-Fock energy E_{HF} obtained in the limit that the basis set approaches completeness [32] by

$$E_{corr} = \mathcal{E}_0 - E_{HF}. \tag{2.2.14}$$

The relative importance of this missing contribution to the energy of the exact solution depends on the system under investigation. Post-Hartree-Fock methods try to recover the correlation energy by refining the Hartree-Fock result by introducing perturbation theory or using more then one determinant to represent the electronic states.

2.3 DENSITY FUNCTIONAL THEORY

In wave-function-based methods, all integral kernels contain the square of the absolute value of the wave function. It follows that this value also contains the information necessary to characterize the system. This argument led to the development of new methods that use the electron density as the underlying physical quantity. They are referred to by the term *Density Functional Theory* (DFT) and are widely used in applications where the exact wave function is not needed [39].

2.3.1 *Electron Density*

In contrast to the wave function of a system, the electron density is a physical entity that can be measured in real systems. When interpreting the square absolute value of the wave function as the probability density for the position of the particles, the electron density $\rho(\mathbf{r})$ at the point $\mathbf{r}$ can be obtained by integrating the probability density $|\psi|^2$ over all spatial and spin coordinates, except the spatial coordinates for one electron, which is then written as

$$\rho(\mathbf{r}_1) = N \int \cdots \int |\psi(\mathbf{x}_1, \mathbf{x}_2, \cdots \mathbf{x}_N|^2 d\mathbf{s}_1 \, d\mathbf{x}_2 \cdots \mathbf{x}_N. \tag{2.3.1}$$

At the positions of the nuclei, the electron density is expected to form a cusp due to the singularity introduced by the factor $-\frac{Z_A}{r_{iA}}$, the coulomb term. The form of this cusp is then related to the charge Z_A of the nucleus. Integrating the electron density over the whole space gives N, the total number of electrons [39][40].

2.3.2 *Hohenberg-Kohn Theorems*

The Hohenberg-Kohn theorems [41] provide a proof to the argument that a formalism using the electron density as the fundamental quantity can be successful. The first theorem proves that the external potential energy term (determined by the charge Z_A and position $\mathbf{R}_A$ of the nuclei) of the Hamiltonian gives rise to a unique wave function and thus electron density for the ground state of the system. The ground state electron density in turn contains, within an additive constant, the external potential energy. These relationships can then be summarized as

$$\rho_0 \Rightarrow \{N, Z_A, \mathbf{R}_A\} \Rightarrow \hat{H} \Rightarrow \psi_0 \Rightarrow E_0 \tag{2.3.2}$$

or by denoting a specific functional, e. g. by writing $E_0[\rho_0]$ to denote the state energy as a functional of the ground state electron density.

Since the ground state energy is a functional of the density,so must be its components [39]. These can be decomposed into the kinetic and potential energy of the electrons independent of the nuclei, T_e and E_{ee}, and a term E_{ext} that encompasses the contributions involving the nuclei, i. e. contributions that are external to the electrons. This can be written as

$$E_0[\rho_0] = T[\rho_0] + E_{ee}[\rho_0] + E_{ext}[\rho_0]. \tag{2.3.3}$$

The functionals $T[\rho_0]$ and $E_{ee}[\rho_0]$ are independent of the nuclei and may be summed up as the Hohenberg-Kohn functional $F_{HK}[\rho_0] = T[\rho_0] + E_{ee}[\rho_0]$, which then results in this expression for the ground state energy functional

$$E_0[\rho_0] = F_{HK}[\rho_0] + \int \rho_0(\mathbf{r}) V_{Ne} d\mathbf{r} \tag{2.3.4}$$

where V_{Ne} is the potential of the Coulomb interaction between the electrons and nuclei. Knowing F_{HK} exactly would make it feasible to solve the Schrödinger equation for arbitrarily large systems exactly. The second of the Hohenberg-Kohn theorems proves that a form of the variational principle also holds for $F_{HK}[\rho]$, where the lowest energy of the system will be delivered if, and only if, the trial density ρ is the ground state density ρ_0.

2.3.3 *Kohn-Sham Density Approach*

Attempts to find an expression for $E_0[\rho_0]$ were made even before publication of the Hohenberg-Kohn theorems and led to the Thomas-Fermi model [39]. However, this model gives only qualitatively correct results for homogeneous metals and fails to predict chemical bonding in molecules. Typically, the biggest contribution to $E_0[\rho_0]$ is the term for the kinetic energy. In wave-function-based methods, the kinetic

energy T can be calculated exactly, which led Kohn and Sham [42] to propose an ansatz where they rearranged the expression for F_{HK} as

$$F_{HK}[\rho_0] = T[\rho_0] + J[\rho_0] + E_{non-cl}[\rho_0], \tag{2.3.5}$$

with the kinetic energy $T[\rho_0]$, the classical Coulomb potential $J[\rho]$, and a catch-all term containing non-classical contributions such as electron exchange and correlation effects.

They were then able to use the expression for the kinetic energy of a Slater Determinant for a reference system of non-interacting electrons

$$T_S = -\frac{1}{2}\sum_i \langle \chi_{i,KS} | \nabla^2 | \chi_{i,KS} \rangle \tag{2.3.6}$$

to approximate the kinetic energy term. The Kohn-Sham orbitals $\chi_{i,KS}$ of this reference system are constructed such that the resulting Kohn-Sham wave function gives the ground state electronic density of the real system:

$$\rho_0(\mathbf{r}) = \sum_i^N \sum_{s\in\{\alpha,\beta\}} |\chi_{i,KS}(\mathbf{r}, s)|^2. \tag{2.3.7}$$

The kinetic energy of this non-interacting system T_0 is not identical to the kinetic energy T for the real system, but since it is possible to express it as a functional of the real electronic density, is is also possible to express the difference between them as a functional. With this partition, Kohn and Sham expressed the functional $F[\rho]$ as

$$F[\rho(\mathbf{r})] = T_S[\rho(\mathbf{r})] + J[\rho(\mathbf{r})] + E_{XC}[\rho(\mathbf{r})], \tag{2.3.8}$$

where the term E_{XC} is called the exchange-correlation energy and is defined as

$$\begin{aligned} E_{XC}[\rho] &= (T[\rho] - T_S[\rho]) + (E_{ee}[\rho] - J[\rho]) \\ &= T_C[\rho] + E_{non-cl}[\rho]. \end{aligned} \tag{2.3.9}$$

The exchange-correlation energy then contains all the contributions to the electronic energy for which an exact form is still unknown.

The Kohn-Sham orbitals are constructed similar to the Hartree-Fock scheme. A one-electron Kohn-Sham operator is defined as

$$\hat{f}^{KS} = -\frac{1}{2}\nabla^2 + \hat{V}_S\mathbf{r}, \tag{2.3.10}$$

using an effective, local potential $\hat{V}_S(\mathbf{r})$. Then, the eigenvalue equations

$$\hat{f}^{KS}\chi_{i,KS} = \epsilon\chi_{i,KS} \tag{2.3.11}$$

are solved. The effective potential V_S is then constructed as the sum of the Coulomb interactions of the electrons with themselves and the nuclei, and the potential leading to the exchange-correlation energy:

$$\hat{V}_S(\mathbf{r_1}) = \int \frac{\rho(\mathbf{r_2})}{r_{12}} d\mathbf{r_2} + \sum_A \frac{Z_A}{r_{1A}} + \hat{V}_{XC}(\mathbf{r_1}), \tag{2.3.12}$$

where the exact form of the term $\hat{V}_{XC}$ is not known, but can be defined as the functional derivative of E_{XC} with respect to the electron density

$$\hat{V}_{XC} \equiv \frac{\delta E_{XC}}{\delta \rho}. \tag{2.3.13}$$

All contributions to the energy except E_{XC} have a known and exact form. All approximations in DFT are introduced by the choice of a suitable functional for the exchange-correlation-energy, and by limiting the basis set for the construction of the Kohn-Sham orbitals [39].

2.3.4 *Time-Dependent Density Functional Theory*

The Hohenberg-Kohn theorems are only valid for the ground state electronic density of the system. Runge and Gross [43] were able to find an extension that is also valid for systems under the influence of time-dependent potential, stating that there is a one-to-one correspondence between time-dependent potentials and electron densities. The theorem can be illustrated by stating that two electron densities $n(\mathbf{r}, t)$ and $n'(\mathbf{r}, t)$ which both arise from a common ground state Ψ_0 at t_0 and evolve under two different potentials $v(\mathbf{r}, t)$ and $v'(\mathbf{r}, t) \neq v(\mathbf{r}, t) + c(t)$, respectively, will become different from each other around t_0 within an infinitesimal time difference [40].

The Kohn-Sham approach requires that a reference wave function of non-interacting electrons can be used to generate the electron density. It can be shown by the van Leuwen theorem that it is also possible to find such a reference for systems where the electron density is time-dependent [40].

These proofs provide the necessary foundation to formulate DFT in a time-dependent manner. Through these formulations, calculation of arbitrary electronic states becomes possible. By considering the linear response of the electron density to an oscillating external potential, it is possible to determine the energy of excited electronic states, which give rise to poles in the response function.

2.4 POST-HARTREE-FOCK METHODS

In wave function-based methods, a general way to recover electron correlation is to use multi-determinantal trial wave functions, where the trial wave function is constructed as a linear combination of Slater determinants

$$\psi = \sum_{i=0} c_i \Psi_i, \tag{2.4.1}$$

where the Ψ_i are Slater determinants constructed from the Hartree-Fock orbitals generated by equation 2.2.13, with $\Psi_0 = \Psi_{HF}$ being the wave function for the ground state and the $\Psi_{i\neq 0}$ are called excited determinants and are constructed by moving an electron from an

occupied orbital of the ground state wave function to an unoccupied one. This ansatz captures the interaction of electronic configurations and is called "Configuration Interaction" (CI) [26].

The inclusion of all possible excited determinants accessible from the Hartree-Fock orbitals generated from a given basis set recovers all the electron correlation accessible via this specific basis set and. This is termed Full Configuration Interaction (FCI). This approach is, however, impractical even for systems of modest size due to the rapid growth of the number of determinants to include. It is thus desirable to limit the number of determinants in 2.4.1 to the ones that have the largest effect on the result. Many schemes for systematic truncation of the number of determinants exist, some of them enabling the use of experience and chemical intuition to pre-select subsets of the complete space of possible determinants.

This truncation however, introduces a size-inconsistency to the method: The energy for a system containing a molecule M twice, at infinite distance, is generally not equal to two times the energy of a system containing the molecule once, so that

$$E(M+M) \neq 2E(M). \tag{2.4.2}$$

This inequality can be made plausible by considering the number of excited states included in the calculation:

Consider a method that includes single and double excitations in the CI-expansion (CISD), used to investigate a system of two molecules $2\,\mathrm{M}=(\mathrm{M_a}+\mathrm{M_b})$ at varying separation distances. CISD would then consider the determinants corresponding to $(\mathrm{M_a}^{**}+\mathrm{M_b})$, $(\mathrm{M_a}^{*}+\mathrm{M_b}^{*})$, and $(\mathrm{M_a}+\mathrm{M_b}^{**})$. At a large separation between $\mathrm{M_a}$ and $\mathrm{M_b}$ where they no longer meaningfully interact, it could be considered to use CISD on a single molecule M and double the resulting energy. That would generate determinants that correspond to the quadruple excitation $(\mathrm{M_a}^{**}+\mathrm{M_b}^{**}$ in the combined $2\,\mathrm{M}$-system that is not considered in the CISD calculation for the combined system [26]. A CISD calculation on a complete system will therefore generally not be identical to the combination of CISD calcualtions of parts of the system, even if they are not interacting.

2.5 MULTICONFIGURATIONAL SELF-CONSISTENT-FIELD

The approach in equation 2.4.1 generates the excited Slater determinants Ψ_i using a set $\{\chi\}$ of molecular orbitals previously generated by another method. It is possible to also make the molecular orbitals $\{\chi\}$ subject to optimization, leading to a method called Multiconfigurational Self-Consistent-Field (MCSCF). Optimizing the orbitals themselves can be termed as "orbital relaxation" in response to the electron correlation introduced by the multiconfigurational approach [26].

2.5.1 *Active Space Methods*

One strategy to limit the number of excited determinants included in equation 2.4.1 is to limit the number of orbitals that may participate in these excitations. The orbitals included in the excitation scheme form a subset called the "Active Space". The simplest method is the "Complete Active Space" (CASSCF) method, which considers all possible excitations within the active space, performing full configuration interaction on the subset [26]. Typically, the frontier orbitals are selected as active space, leading to a basic nomenclature for the size of an active space as (e, o), where e and o are the number of electrons and orbitals in the active space, respectively [44]. Some publications also use square brackets to denote the active space [26], i. e. "[6,7]-CASSCF". In this thesis, the round form will be used. Figure 2.1 shows a representation of a (6,7) active space.

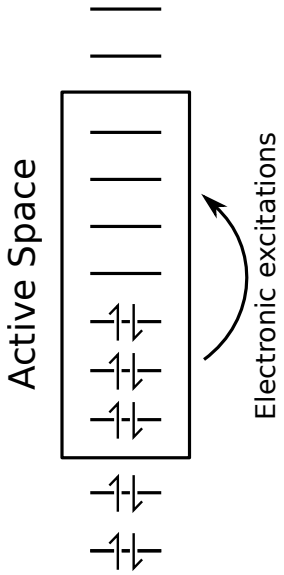

Figure 2.1: Schematic representation of an active space.

Active Space Selection

Selection of a suitable active space depends on the chemical question to be answered; thus, it is a subjective process that requires experience and chemical intuition. However, some general "rules of thumb" can be formulated to aid the selection [26].

1. For a given occupied orbital to include in the active space, if there is a corresponding unoccupied orbital, both orbitals will should be included.

2. The frontier orbitals, i. e. the highest occupied and lowest unoccupied orbitals generated by a Hartree-Fock method typically provide the highest contributions.

3. When the geometry of the molecule changes, i. e. during a chemical reaction, the contribution of a particular orbital to the correlation energy will also change. The active space should thus include orbitals that may become important during critical process phases, such as transition states and changes in orbital character.

4. Analyzing occupation numbers of orbitals gained from previous correlated methods may reveal if the inclusion is justified. Orbitals that are almost completely filled or empty typically contribute less to the correlation effects than partially filled orbitals.

Orbitals representing the inner shell of atoms with very low orbital energies are expected to make only negligible contributions to the configuration interaction, and to change very little under orbital optimization. It is thus possible to exclude these orbitals from the orbital re-optimization The excluded orbital are then called "frozen" orbitals [44].

2.5.2 *State Averaging*

When calculating excited electronic states and aiming to accurately recover the transition dipole moments for the excitations, it is necessary to keep the wave functions strictly orthogonal. This is done by optimizing several states at once with the same orbitals, which then describe the corresponding electronic states equally well. This method is called "state averaging" [45]. We define an energy function as a linear combination of the energies of the individual states $|I\rangle$

$$E = \sum w_I E_I, \tag{2.5.1}$$

where the w_I are constant weight parameters [46].

2.6 DENSITY MATRIX RENORMALISATION GROUP

The selection of active spaces is necessarily a subjective matter. There is no simple and obvious way to methodically improve the accuracy of the results of a multi-configurational method, aside from increasing the space itself, which comes at an exponential increase of computational cost. There is a desire to find methods that can be tuned according to available computational resources and required accuracy by using a limited number of parameters. If these parameters were to influence the performance of the method in a predictable manner, it would be

possible to create black-box methods and thereby simplify the usage of electron correlation methods.

A promising candidate to fill this role is the Density Matrix Renormalization Group (DMRG) method. It was developed to solve correlated quantum problems in condensed matter physics [47], has been adapted for quantum chemical problems [48] and successfully used to treat electron correlation in transition metal complexes [49][50].

2.6.1 *DMRG Algorithm*

The formalism given in this section is taken from Wouters and van Neck [20]. The ansatz of 2.4.1 is transformed into a product of tensors, called a "tensor train". These tensors are then simplified by data-reduction techniques, typically by truncated singular value decomposition (SVD). The transformation proceeds by interpreting the factors c_i as a tensor $C^{\{n_i\}}$ of rank L, where L is the number of spatial orbitals included in the active space and n_i denotes the number of electrons occupying orbital i, as one of $\{—, \uparrow, \downarrow, \uparrow\downarrow\}$. The tensor $C^{\{n_i\}}$ can be exactly decomposed by an SVD so that

$$C^{n_1;n_2\cdots n_L} = \sum_{\alpha_1} U[1]_{n_1;\alpha_1} s[1]_{\alpha_1} V[1]_{\alpha_1;n_2\cdots n_L}. \tag{2.6.1}$$

This decomposition can then be repeated for $V[1]$, giving

$$V[1]_{\alpha_1 n_2;n_3\cdots n_L} = \sum_{\alpha_2} U[2]_{\alpha_1 n_2;\alpha_2} s[2]_{\alpha_2} V[2]_{\alpha_2;n_3\cdots n_L}. \tag{2.6.2}$$

By continuing this process for all n and absorbing the $s[n]$ into one of the two adjacent tensors giving $A[n]$, the single tensor $C^{\{n_i\}}$ of rank L is exactly decomposed into L tensors of rank 2 and 3, showing the sequential nature of the tensor train:

$$C^{n_1 n_2\cdots n_L} = \sum_{\alpha_1,\alpha_2,\cdots\alpha_{k-1}} A[1]^{n_1}_{\alpha_1} A[2]^{n_2}_{\alpha_1;\alpha_2} \cdots A[L-1]^{n_{L-1}}_{\alpha_{L-2};\alpha_{L-1}} A[L]^{n_L}_{\alpha_{L-1}}. \tag{2.6.3}$$

Optimizing the elements of c_i in equation 2.4.1 with respect to the energy is equivalent to optimize the tensors $A[n]$.

In the exact decomposition, the number of elements contained in the indices α_k and thus the tensors $A[k]$ grows exponentially towards the middle of the decomposition, such that $dim(\alpha_k) = min(4^k, 4^{L-k})$. However, the SVD offers a straightforward path to an approximation technique, where only the m most significant values are kept in the α_k indices. This transformed and truncated ansatz is then called a Matrix Product State (MPS), the truncation constant m is called the bond dimension. The MPS can be optimized by the DMRG algorithm, yielding a variational upper bound for the ground state energy [20].

In the quantum chemical formulation of DMRG, the MPS is constructed by assigning the molecular orbitals of the active space to the indices n_k, which are then called a site. Since the decomposition is truncated, the order of the orbitals along the 1D-lattice of the MPS has an effect on the resulting approximation. The optimization then proceeds in macro-iterations called sweeps, consisting of micro-iterations. In a micro-iteration, two adjacent sites are contracted along their shared bond index into a single two-site tensor,

$$\sum_{\alpha_i} A[i]^{n_i}_{\alpha_{i-1};\alpha_i} A[i+1]^{n_{i+1}}_{\alpha_i;\alpha_{i+1}} = B[i]^{n_i;n_{i+1}}_{\alpha_{i-1};\alpha_{i+1}}, \tag{2.6.4}$$

which is optimized to give the lowest ground state energy with a local effective Hamiltonian. The optimized tensor is then decomposed again by a truncated SVD. In the next micro-iteration, the index i moves one step and the process is repeated. A full sweep consists of moving the index i along the train once in each direction, reversing at the end. The algorithm ends after a set number of sweeps or convergence criteria.

2.6.2 *Orbital Entanglement*

The MPS ansatz offers methods to analyze the resulting wave function in terms of the contribution of orbitals to the active space. Derived from to the density matrix

$$\rho = |\Psi\rangle \langle\Psi| \tag{2.6.5}$$

for the complete wave function, a reduced density matrix $\hat{\rho}^S$ can be constructed for a subsystem of the active space [20]. The active space may be partitioned into the subsystems P and Q, consisting of the orthonormal basis states $\{|P_i\rangle\}$ and $\{|Q_j\rangle\}$, respectively. Then, the complete system is described by the product space $\{|P_i\rangle\} \otimes \{|Q_j\rangle\}$ and wave functions of the form $|\Psi\rangle = \sum_{ij} C_{ij} |P_i\rangle |Q_j\rangle$. Performing an SVD on the matrix C leads to

$$\begin{aligned} |\Psi\rangle &= \sum_{ij} C_{ij} |P_i\rangle |Q_j\rangle \\ &= \sum_{ijk} U_{ik} \sigma_k V_{kj} |P_i\rangle |Q_j\rangle \\ &= \sum_{k} \sigma_k |\tilde{P}_i\rangle |\tilde{Q}_j\rangle . \end{aligned} \tag{2.6.6}$$

A reduced density matrix ρ^P for subsystem P can then be formed by taking the partial trace with respect to Q, as

$$\begin{aligned}\rho^P &= \mathrm{Tr}_Q(\rho) \\ &= \sum_j \langle Q_j|\Psi\rangle \langle\Psi|Q_j\rangle \\ &= \sum_{ijl} |S_i\rangle C_{ij} C^\dagger_{jl} \langle S_l| \\ &= \sum_k |\tilde{S}_k\rangle \sigma_k^2 \langle\tilde{S}_k| .\end{aligned} \tag{2.6.7}$$

From these σ_k^2, the *von Neumann entropy* S with respect to P and Q can be calculated as

$$S = -\sum_k \sigma_k^2 \ln \sigma_k^2, \tag{2.6.8}$$

where, for normalized $|\Psi\rangle$,

$$\sum_k \sigma_k^2 = 1. \tag{2.6.9}$$

The von Neumann entropy is a measure of how entangled P and Q are. If they are not entangled at all, i. e. when $\sigma_1 = 1$ and $\sigma_{k\neq 1} = 0$, $S = 0$. If all states are equally entangled, with $\sigma_i = \sigma_k$ for all i and k, then the entropy is at a maximum at $S = \ln(L_{min})$ where L_{min} is the minimum of the number of states in P and Q. Now, a single-orbital entropy $s(1)_i$ and two-orbital entropy $s(2)_{ik}$ can be defined, where the subsystem P consists of the orbital i or the orbitals i and j, respectively, and Q contains all other orbitals.

For two orbitals i and j, the sum of their single-orbital entropies is equal to or greater than the two-orbital entropy of both combined, with

$$s(1)_i + s(1)_j \geq s(2)_{ij}. \tag{2.6.10}$$

The difference $s(1)_i + s(1)_j - s(2)_{ij}$ can be interpreted as the amount of entanglement between i and j: The single-orbital entropy gives, for each of the orbitals, the entanglement with the environment, including the other orbital. Subtracting the two-orbital entropy then leaves the entanglement between the two orbitals, leading to the definition of the *mutual information* between two orbitals

$$I_{i,j} = \frac{1}{2}(s(1)_i + s(1)_j - s(2)_{ij})(1 - \delta_{ij}), \tag{2.6.11}$$

which was proposed by Rissler, Noack and White [51] (as cited in [20]) as a measure for ordering the orbitals inside the active space.

2.6.3 *Orbital Ordering*

The DMRG method was conceived from the analysis of real systems with close-range interactions, where the sites in the algorithm would

be ordered to reflect their spatial arrangement, e. g. creating a one-dimensional lattice. For molecular orbitals, no preferred ordering is immediately obvious. Indeed, the ordering of the orbitals is crucial for the performance of the method, where improper orderings may lead to slow convergence or trapping the algorithm in local minima.

It has been shown that reordering strongly interacting orbitals to the center of the lattice is beneficial [52]. This process can be canonized in various ways, e.g. by analyzing the mutual information matrix. If this matrix is taken as a connectivity matrix for a complete graph, this graph produces an entanglement diagram. The Fiedler vector, i. e. the eigenvector of the second smallest eigenvalue of the graph Laplacian for this connectivity matrix, has been shown to be a promising candidate for a canonical ordering of orbitals [49][53].

3

COMPUTATIONAL METHODS AND DETAILS

This chapter gives an overview of the steps taken in the analysis, and lists the computer programs and principal parameters used.

The equilibrium geometry of the molecule, i. e. the coordinates of the atoms for which all normal modes for nuclear oscillations are at their minimum potential, was calculated using the Gaussian 16 program [54]. A geometry optimization algorithm was used, employing DFT with the B3LYP functional [55] with a def2-TZVPP basis set [56]. The starting geometry was a best guess based on common bond lengths and is given in appendix A.1.1.

Excited electronic states at the equilibrium geometry were computed using two methods. The first employs TD-DFT, with the def2-TZVPP basis set and B3LYP functional, and the second employs the DMRGSCF method where the orbitals are optimized as well, and the ANO-RCC-MB basis set [57] with an implicit relativistic Douglas-Kroll-Hess Hamiltonian operator [58]. The DMRGSCF calculation was performed using the QCMaquis 2.1 suite [59][60], interfaced to the OpenMolcas 18.09 program [61]. The m-parameter used for this analysis was chosen to be 1000.

To analyze the character of the electronic transitions, the TheoDORE program [62] was used to compute and localize the shift in electron density between molecular fragments in response to the electronic excitations.

The wave functions given as matrix product states produced by the DMRG procedure were analyzed using the SCINE Autocas program [63][64][65][66].

To investigate the ligand dissociation behavior, molecular geometries were created where either the NO fragment, one of the CO fragments, or both the NO and a CO fragment, were shifted along their respective bonds with the Mo-center. The displacement of the ligands from the equilibrium geometry ranged from a bond compression of -0.4 Å to an elongation of 50 Å. The list of intermediate steps is given in appendix A.2.

At these geometries, computations were performed using DMRG-CI without optimizing the orbitals, i. e. optimizing the CI-coefficients only. The m-parameter was chosen to be 250 for the bond elongation analysis. The starting orbitals for the DMRG computations were generated by computing the Hartree-Fock orbitals for that molecular geometry, using the orbital expansion coefficients from the previous geometry as an initial guess for the orbitals in the Hartree-Fock procedure. All

DMRG calculations used an orbital ordering according to increasing orbital energy.

3.1 DMRG ORBITAL SELECTION ALGORITHM

To reduce the active space used in the DMRG calculations, the algorithm proposed by Stein and Reiher [67] was used and extended for excited states. The extension uses state-specific values for the single-orbital entropy $s(1)_{i,S}$ and the mutual information $I_{ij,S}$ (see section 2.6.2) for each electronic state S. Then, across all states under consideration, the maximum value for each orbital or pair of orbitals is determined as

$$s(1)_{max,i} = \max_S s(1)_{i,S} \tag{3.1.1}$$

and

$$I_{max,ij} = \max_S I_{ij,S}. \tag{3.1.2}$$

The $s(1)_{max,i}$ and $I_{max,ij}$ are then used in the algorithm given in [67], giving the procedure delineated[1] in algorithm 1.

Algorithm 1: Orbital selection procedure for state-averaged DMRG calculations

```
choose an initial, big active space O;
run an initial DMRG sweep (DMRG-CI only) calculation;
calculate s(s)_max,i and I_max,ij;
if max(s(1)_max,i > 0.14 then
    if plateaus in distribution of s(1)_max,i then
        reduce O to contain the orbitals on the highest plateau(s)
    else
        remove orbitals from O where
          s(1)_max,i < 1 − 2%  max(s(1)_max,i)
    end
    use O for the CASSCF or DMRG-SCF calculation
end
```

1 Algorithmic notation was prepared by Dr. Markus Oppel.

4 RESULTS AND DISCUSSION

This section presents the calculation results and discusses them. A reference geometry for the complex will be described, which was used to analyze the electronic excited states and as a starting point to investigate the dissociation behavior of the CO and NO ligands.

4.1 EQUILIBRIUM GEOMETRY

Initial assessment of the geometry of the molecule concerned the configuration of the four ligands. Cyclopentadienyl (Cp) is a tridentate *fac*-coordinating ligand. Adding two CO and one NO ligand leads to a formally octahedral complex, with the three smaller ligands coordinated opposite to the Cp-ring. Chemical intuition suggests the molecule will form a symmetric complex, where the Cp-ring in the equilibrium geometry is arranged in either a *staggered* or *eclipsed* conformation relative to NO, as symbolized in Figures 4.1a and 4.1b respectively. Both conformations lead to an overall C_S-symmetry, which will be used by the geometry optimization algorithms.

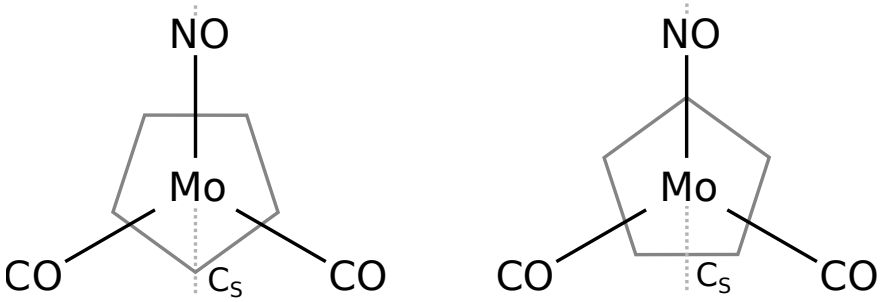

(a) Cp-ring with CH-groups staggered with respect to NO.

(b) Cp-ring with one of the CH-groups eclipsed by NO.

Figure 4.1: Projection of staggered 4.1a and eclipsed 4.1b conformations of the Cp-ring with respect to the NO ligand. The dotted gray line represents the C_S-plane

The geometry optimization procedure used is sensitive to the initial guess geometry. Initial exploratory calculations[1] with an eclipsed conformation guess at the B3LYP/def2-SVP level of theory were performed and analyzed to find the correct conformation for the Cp-ring. Vibrational analysis for the eclipsed geometry revealed a negative frequency of $17\,cm^{-1}$ for the normal mode that corresponds to a rotation of the Cp-ring. This indicates that such a rotation is required to find

1 Initial geometry optimizations were performed by Dr. Markus Oppel

the true equilibrium geometry. This was confirmed by a geometry optimization at the B3LYP/def2-TZVPP level, using an initial geometry guess (given in appendix A) featuring a staggered conformation. The resulting optimized geometry is given in Figure 4.2.

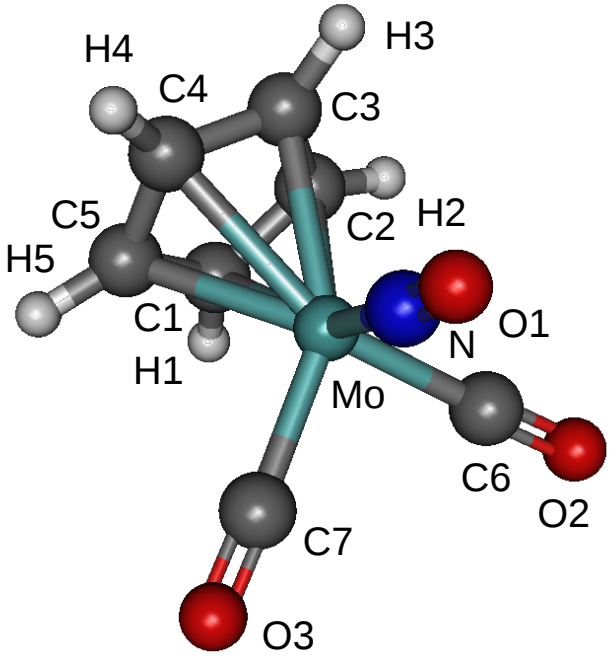

Figure 4.2: Equilibrium geometry of the complex, with atoms labeled.

4.1.1 *Vibrational Analysis*

Vibrational analysis on the staggered geometry showed no negative frequencies. In Table 4.1, frequencies for the stretching modes of the CO and NO ligands are compared to experimental data from Schwalbe et al. [68], and selected frequencies for vibrations of the Cp-ring are compared to experimental data from Parker and Stiddard [69]. The calculated oscillator strengths are also given. The computed frequencies and intensities were convoluted using Lorentzian functions with a full width at half maximum of 98 cm^{-1} to give a visual, intuitive impression of the predicted spectrum under experimental conditions, and the result is displayed in Figure 4.3.

The frequency analysis uses the second derivative of the energy with respect to displacement of the atoms along each vibrational normal mode. This approximates the potential energy experienced by the nuclei as a harmonic well, typically leading to a systematic overestimation of the frequencies, whereas in the real system, the nuclei experience an anharmonic potential. The frequencies shown in

Table 4.1: Experimental and calculated infrared frequencies, given in cm^{-1}. The values in parentheses are the oscillator strengths for the calculated frequencies, given in arbitrary units.

Mode	Exp. [68] /cm^{-1}	Calc. / cm^{-1}	Int. (Arb. Units)	Type
ν (NO)	1663	1772	(1252)	str.
ν_A (CO)	1937	2018	(1164)	str. asym.
ν_S (CO)	2020	2082	(738)	str. sym.
Mode	Exp. [69] /cm^{-1}	Calc. / cm^{-1}	Int. (Arb. Units)	Type
ν_1 (Cp)	3112	3256	(0.52)	CH-str.
ν_3 (Cp)	1106	1134	(0.44)	Ring breath.
ν_5 (Cp)	3112	3246	(0.11)	CH-str.
ν_9 (Cp)	3112	3233	(0.07)	CH-str.
(not observed)		3232	(0.00)	CH-str.

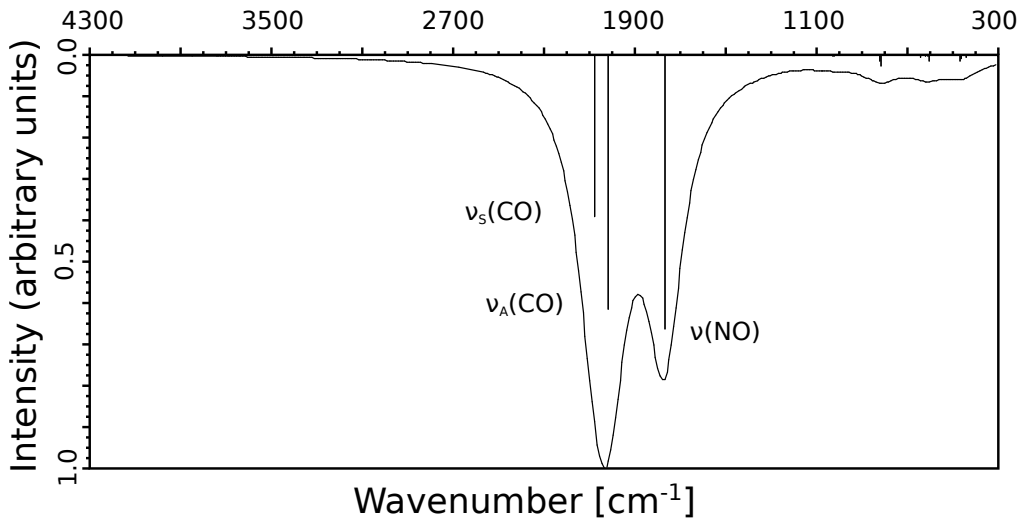

Figure 4.3: Calculated infrared absorption spectrum obtained by convolution of the vibrational frequencies with Gaussian functions of a full width at half maximum of 98 cm^{-1}.

Table 4.1 show that the experimental frequencies are lower by factors between 0.976 and 0.938. The Computational Chemistry Comparison and Benchmark Database [70] provides a range of empirical factors for scaling purposes and gives a range of 0.963 ± 0.044 for the B3LYP/def2-TZVPP level of theory. The computed factors for the complex thus are in the expected range.

Parker and Stiddard [69] report that the signals for the CH-stretching modes could not be resolved for most of the Cp-containing complexes they investigated. While the frequencies calculated for these modes might allow separate detection, the estimated intensities suggest that the ν_5 and ν_9 modes may be too weak to detect. Vibrations that are infrared-inactive in the local C_{5V} symmetry of the Cp-ring are expected to have equivalent vibrations of low intensity in the complex, if the local symmetry is only weakly perturbed. In particular, the equivalent of the normal mode ν_9 belongs to the infrared-inactive vibration e_2. The low calculated intensity is in agreement with this.

4.1.2 *Bond Geometry Analysis*

Some features of the geometry can be compared to experimental data published by Schwalbe et al. [68], which are given in Table 4.2. The calculated values for these features come to within 2 % of the experimental values, except for the direct distances between Mo and the CO and NO ligands, which are within 5 % of the experimental values. The angle $\angle$ Mo−N−O is of particular interest, as it is an indicator for the oxidation state of NO. Linearly bound NO can be treated as NO^+, while attachment at an obtuse angle is considered to indicate an NO^- species [71]. The excellent agreement between the experimental and the calculated attachment angle gives confidence that our computation has arrived at a geometry with the correct structural features.

There arise, however, two issues from the comparison to the experimental data of Schwalbe et al. [68] that need to be addressed. From the crystallographic data, the C_S symmetry seems to be slightly broken by small, but significant differences in the CO bond geometry relative to Mo and NO, and in the C−O distance. It seems possible that these deviations are the result of the crystalline environment in the solid phase, whereas the quantum chemical calculations were performed without a chemical environment. Secondly, since it is not possible to reliably differentiate C from N by x-ray crystallography, Schwalbe et al. used their own quantum chemical calculations to support their assignment of NO and CO. This precludes the use of their assignment as the sole benchmark for other chemical calculations presented in this work. The linear attachment of the NO ligand is, however, strongly supported by their data.

Table 4.2: Experimental and calculated geometry features of the molecule. Distances are given in [Å], angles in [°].

Feature	Exp.[68]	Calc.
Mo−N	1.899	1.812
Mo−C6	1.941	1.996
Mo−C7	1.957	1.996
∠ Mo−N−O	177.85	176.27
N−O	1.167	1.17
∠ Mo−C−O	178.21	177.91
	176.80	177.91
C−O	1.143	1.146
	1.154	1.146
∠ N−Mo−C6	91.35	91.81
∠ N−Mo−C7	91.79	91.81

4.2 EXCITED STATES

For the optimized geometry, the excited electronic states were investigated using time-dependent density functional theory (TD-DFT). The corresponding differences in electron density were then analyzed to give an indication of the nature of the excitation. From this analysis, a number of excited states of interest were determined. On these excited states, further analysis was carried out using the DMRG method.

4.2.1 *TD-DFT Excited States and Analysis*

For the optimized geometry described above, excited states were calculated using the TD-DFT method at the B3LYP/def2-TZVPP level of theory. Thirty excited singlet and triplet states each were calculated. Excitation energies and oscillator strengths for the singlet states are given in the appendix in Table A.2. From these values, an UV-Vis spectrum was generated by convolution with a Gaussian function, given in Figure 4.4.

Of the lower-lying states, the excited singlet states four, six, and seven show appreciable oscillator strengths. The oscillator strength is proportional to the probability of absorbing a photon of suitable energy. This marks them as states that merit further investigation, to analyze if the molecule can undergo dissociative processes from excitations to one of these states.

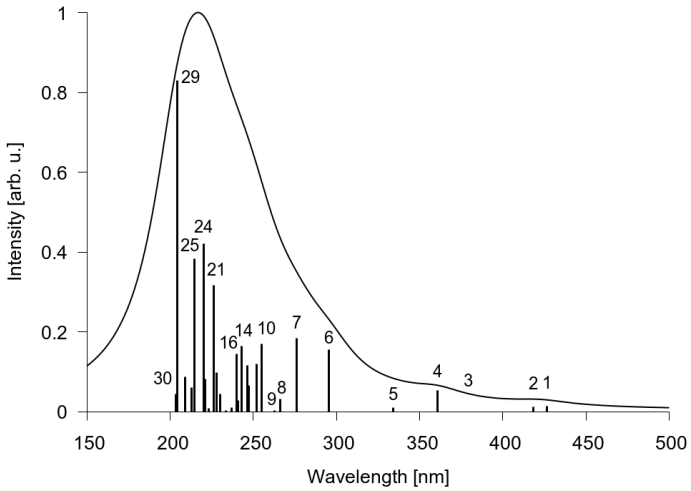

Figure 4.4: Position and relative intensity of the 30 lowest electronic singlet states as stick spectrum, with the resulting spectrum from convolution with a Lorentzian function with a half-width of 20 nm.

Analysis of Excited States

To make efficient use of the computationally more demanding DMRG method, it is desirable to pre-select a limited number of excited states of interest. We analyzed the nature of the excited states to aid in the selection process. Their electron density was compared to the density of the ground state, using the TheoDORE program package [62]. By partitioning the molecule into fragments, it is possible to determine the effect of the electronic excitation with respect to the transfer of charge from one fragment of the molecule to another. The molecule was subdivided into one fragment for each of the ligands and an additional fragment for the Mo-center. In the context of organometallic and inorganic complex chemistry, this allows for characterization of the excited states by their charge-transfer character.

Ligand dissociation is typically mediated by population of antibonding or depopulation of bonding orbitals between the metal center and its ligands. The resulting shift in electron density can be described as a charge transfer, so it is desirable to include states showing charge transfer to or from the ligands (metal-ligand or ligand-metal charge-transfer - MLCT or LMCT). Figure 4.5 shows the overall charge transfer character of the first 30 excited electronic singlet states and Figure 4.6 divides these categories according to the participating ligands, and, in the case of ligand-to-ligand charge transfer (LLCT), by the ligand to which the electron density is transferred to. Charge transfer within a fragment is given as metal-centered (MC) or inter-ligand (IL) character.

The first five excited states show the smallest amount of ligand-metal charge transfer, and the next five states show double the amount of LMCT character. State seven is the first of the states with appreciable

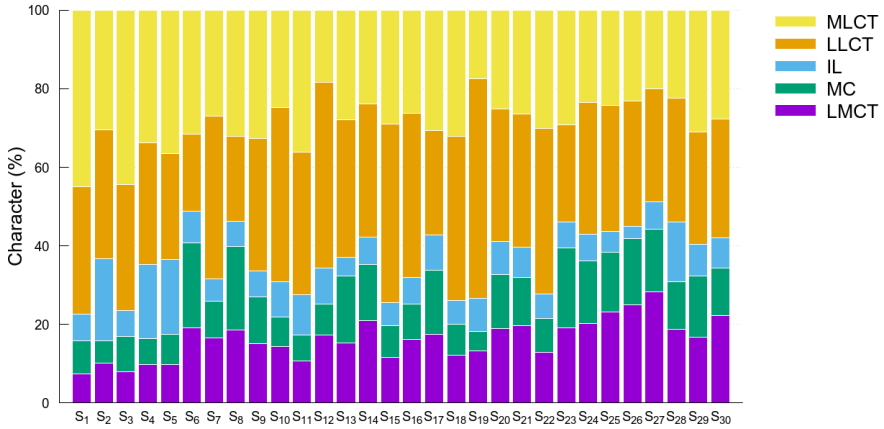

Figure 4.5: Charge-transfer character of the first 30 excited electronic singlet states.

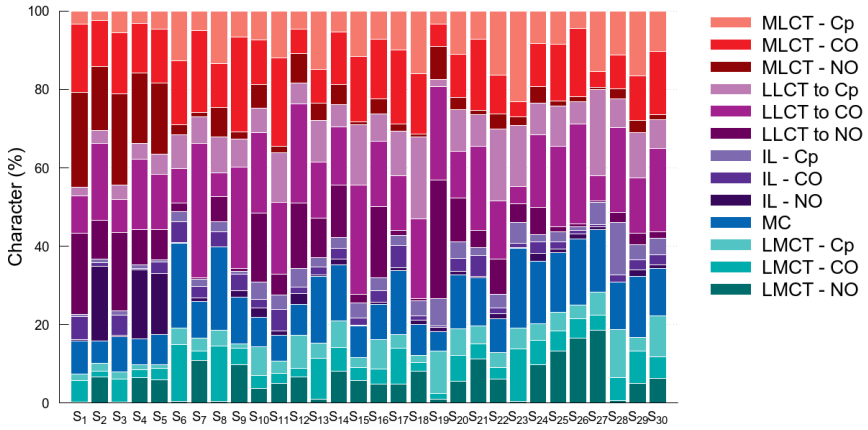

Figure 4.6: Detailed charge-transfer character of the first 30 excited electronic singlet states, further separated by participating ligand. For ligand-to-ligand charge transfer, the ligand receiving additional electron density is noted.

oscillator strength that has only a small contribution of metal- and ligand-centered excitation, which means that it might be of particular interest for population and depopulation of orbitals.

In a detailed analysis that takes into account the particular fragments, the first five excited states show intense participation of the NO ligand, in particular a charge transfer from the metal center to NO. This is contrasted by very little participation of NO in states six to nine. In these states, the CO ligands show a larger participation. This is an indicator for possible selective dissociation of either of these ligands, mediated by these states. Charge transfer involving the Cp ring becomes noticeable in states six and eight, but otherwise only plays a minor role up until state eleven.

To investigate the selective photo-dissociation behavior of NO and CO, the states four, six, and seven are promising candidates to include. Including more excited states would of course provide opportunities for a more detailed analysis. However, due to the computational demand of the DMRG method, it is necessary to limit the scope to the minimum number of states required to answer the question at hand. Thus, in the following analysis, only the ground state and first seven excited electronic singlet states will be included.

4.2.2 *Determining the DMRG Active Space*

When using multiconfigurational methods, the selection of the active space takes an important role. A set of molecular orbitals calculated at the HF/ANO-RCC-MB level, described in Table A.4, was used as the starting point for the DMRG method. The selection process consisted of a first guess for the active space based on chemical intuition, which is then refined by analyzing the mutual information.

In the first step of selecting the active space, the lowest 20 molecular orbitals which are localized around the non-hydrogen atoms and correspond to their low-lying core orbitals, were excluded from the optimization process by fixing their coefficients - similar to a "frozen-core" approach [26]. This included the $1s$-orbitals for all non-hydrogen atoms and up to the $3p$-orbitals for Mo.

Then, from the remaining occupied, non-frozen orbitals, the following were excluded from the active space in a first trial:

- the $3d$-, $4s$ and $4p$-orbitals of Mo,
- the first σ- and corresponding $\sigma*$-orbitals of CO and NO, and
- the first six σ-orbitals of the Cp-ring.

All 19 remaining occupied orbitals, containing 38 electrons, were then included in the active space. From the virtual orbitals, those with a complementary antibonding character to the bond-forming molecular orbitals were added the active space, up to and including

the molecular orbital 71. Orbital 71 also contains the first Rydberg *s*-orbital. The preliminary (38, 30) active space then consisted of the molecular orbitals 42 to 71.

With these orbitals and active space, the first eight electronic states were calculated using the DMRG-CI method with an m-parameter of 1000. The resulting orbital entanglement was analyzed to identify orbitals that have only small, negligible interactions within the active space. To make sure that the entanglement of all selected electronic states is considered, for each state-specific $s(1)_{i,S}$ and $I_{ij,S}$ given state S, the maximum value encountered over these states was taken as the overall value.

The values for the mutual information between two orbitals $I_{ij,S}$ and the single-orbital entropy $s(1)_{i,S}$ for a specific state S were reduced by taking the maximum of the values with respect to all states, such that

$$\begin{aligned} I_{max,ij} &= \max_S I_{ij,S}, \\ s(1)_{max,i} &= \max_S s(1)_{i,S}. \end{aligned} \tag{4.2.1}$$

The resulting diagram showing $I_{max,ij}$ and $s(1)_{max,i}$ is given in Figure 4.7.

The preliminary entanglement diagram shows that four of the included σ^*-orbitals of the Cp ligand do not exhibit appreciable entanglement in any of the electronic states analyzed. This is in accord with chemical intuition, as the seven excited states under consideration did not show participation of the Cp-ring in the charge-transfer analysis of section 4.2.1. Therefore, the σ^*(Cp)-orbitals were excluded from the active space.

The calculation was then repeated using the smaller (30, 26) active space, and including orbital optimization in the algorithm. The resulting reduced entanglement diagram is given in Figure 4.8. In this diagram, all orbitals contribute an appreciable amount of single-orbital entropy and show entanglement with other orbitals. The π(Cp)-orbital 53 and Rydberg s-orbital would be candidates for further reduction of the active space, should the need arise.

The values for $s(1)_{max,i}$ for both the initial (38, 30) and reduced (30, 26) active spaces are given in table 4.3 as percentage of the highest value for the given state. The complete data for the $s_i(1)$ is given in the appendix. The procedure proposed by [67] recommends removing orbitals that show a relative single-orbital entropy of less than 2 % of the orbital with the highest single-orbital entropy. Thus, the removal of the σ^*(Cp)-orbitals is in line with the recommended procedure.

4.2.3 *DMRG Excited States Results*

The calculations in section 4.2.2 yielded energies for the electronic states. Table 4.4 compares the excitation energies to those calculated

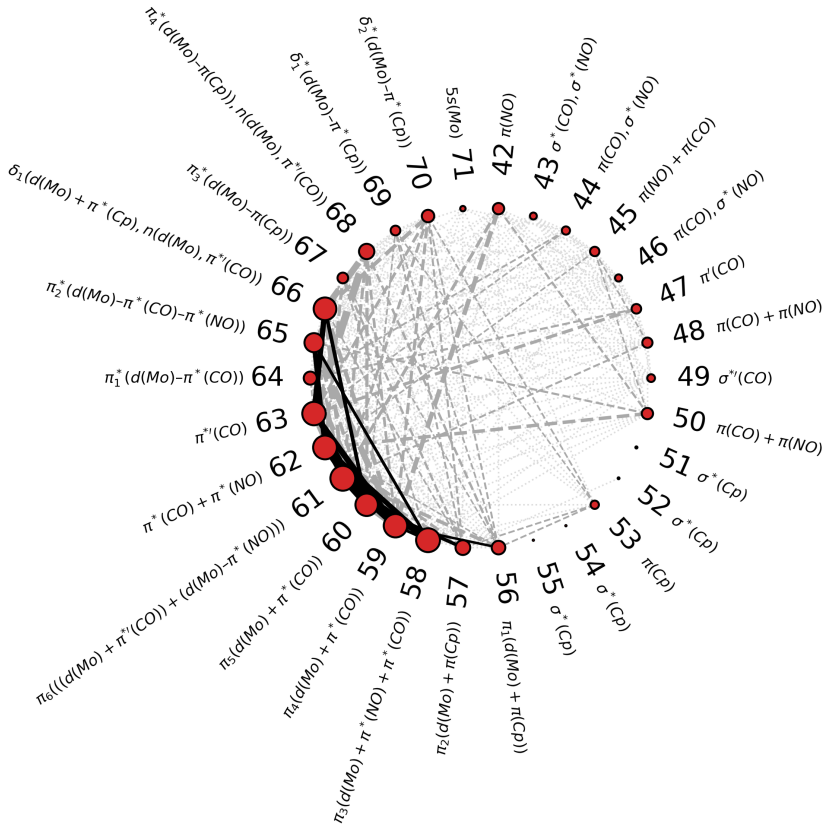

Figure 4.7: Entanglement diagram for the initial (38, 30)[1000] guess for the active space, as a combination of the correlation diagrams of the first eight electronic states. Each line represents the maximum of the mutual information between two orbitals encountered over all eight states.

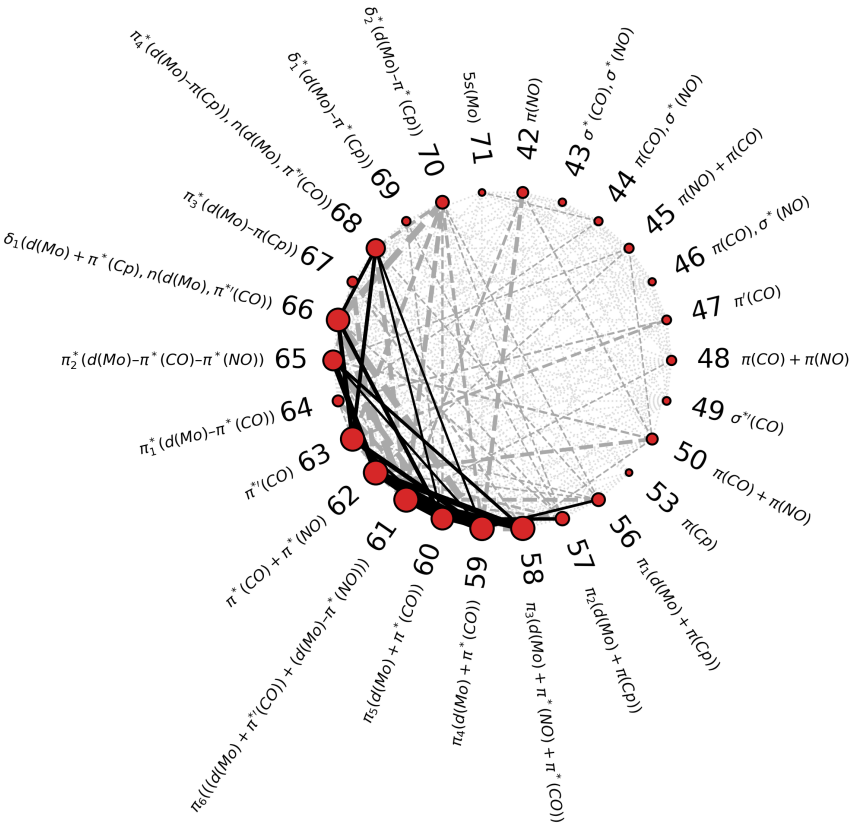

Figure 4.8: Entanglement diagram for the reduced (30, 26)[250] active space, as a combination of the correlation diagrams of the first eight electronic states.

Table 4.3: Relative maximum single orbital entropy $s(1)_{rel}$ for the initial and reduced active space, as percentage of $s_{max,i}(1)$ compared to the largest value of $s_{max,i}(1)$ for each active space.

CAS-(38, 30)		CAS-(30, 26)	
Orbital Nr.	$s(1)_{rel}$ /[%]	Orbital Nr.	$s(1)_{rel}$ /[%]
61	100.00	61	100.00
58	92.20	62	97.64
62	91.84	59	95.20
63	89.14	63	94.09
59	88.92	58	93.98
66	83.15	66	88.75
60	81.70	60	81.84
65	58.85	65	68.27
68	37.94	68	58.03
57	35.16	57	31.33
56	29.97	56	28.46
64	27.74	70	28.16
70	24.97	50	21.02
42	20.77	64	20.78
50	20.58	42	20.69
67	18.38	67	18.34
48	16.84	48	15.01
69	15.20	45	14.53
47	14.84	47	13.55
45	14.22	69	12.31
53	11.19	44	11.62
44	10.84	49	10.37
49	9.69	43	9.46
46	8.26	46	9.07
45	14.22	69	12.31
53	11.19	44	11.62
44	10.84	49	10.37
49	9.69	43	9.46
46	8.26	46	9.07
43	7.86	53	7.67
71	4.72	71	7.65
51	0.70		
52	0.57		
54	0.27		
55	0.26		

Table 4.4: Excitation energies for the first seven electronic singlet states compared between TD-DFT and DMRG calculations; using the larger active space and only optimizing the CI-coefficients (DMRG-CI), and using a reduced active space and optimizing the orbitals as well (DMRGSCF).

	Excitation Energies /eV		
State	TD-DFT	DMRG-CI(38,30)[1000]	DMRGSCF(30,26)[250]
S_1	2.91	3.09	3.22
S_2	2.96	3.36	3.27
S_3	3.27	3.36	3.45
S_4	3.44	3.97	4.03
S_5	3.71	3.99	4.18
S_6	4.20	5.07	5.22
S_7	4.49	5.33	5.53

by the TD-DFT method above as described in section 4.2.1. No experimental data are available to give context to these values, but the excitation energies given by TD-DFT are consistently smaller than for the same state calculated using DMRG.

The absolute energy obtained for the reduced active space calculation is 0.70 eV lower than the preliminary guess, which, since the method conforms to the variational principle, gives confidence that the reduction of the active space is acceptable: If the order were reversed so that the gains of optimizing the orbitals were offset by losses due to the reduction of the active space, the reduction would need to be re-examined.

4.2.4 *Benchmarking DMRG for Excited States*

For analysis of the dissociation behavior, the electronic energy has to be calculated at different molecular geometries. This multiplies the computational cost by the number of desired geometries. As the calculation of eight electronic states described above in section 4.2.3 consumed over 4000 core-hours[2] over the course of 11 days, benchmarking of the DMRG method for the molecule was performed to find a balance between calculation quality and available computational resources.

We used the same reduced (30,26) active space and equilibrium geometry of the molecule as above for benchmarking, but only two electronic states were calculated. The m-parameter was varied in the

2 On 16 cores of an Intel(R) Xeon(R) Gold 6138 CPU

range from 10 to 300. Each benchmark calculation was performed on ten cores of an Intel(R) Xeon(R) E5-2650 v3 CPU. Figure 4.9 shows the dependence of the electronic ground state energy on the m-parameter. Figure 4.10 shows the dependence of the time taken for the first two iteration steps and the time taken for the completion of the algorithm on the chosen m-parameter.

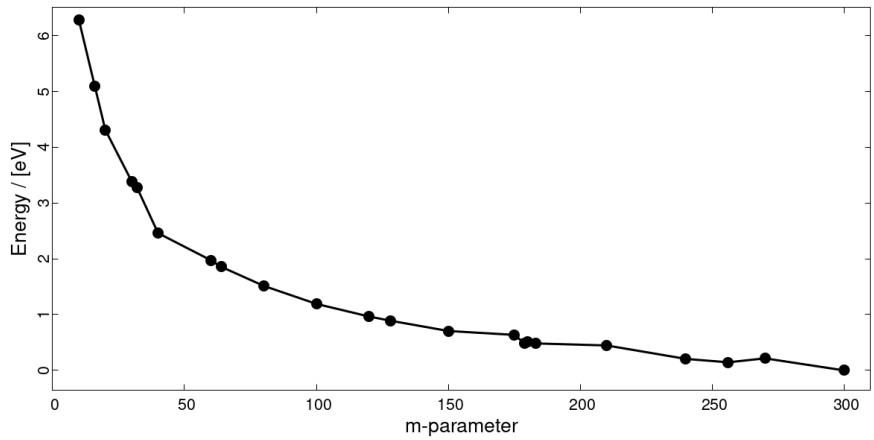

Figure 4.9: Energy of the molecule's electronic ground state calculated with DMRGSCF, dependent on the m-parameter. The energy is given relative to the energy for the highest m-parameter.

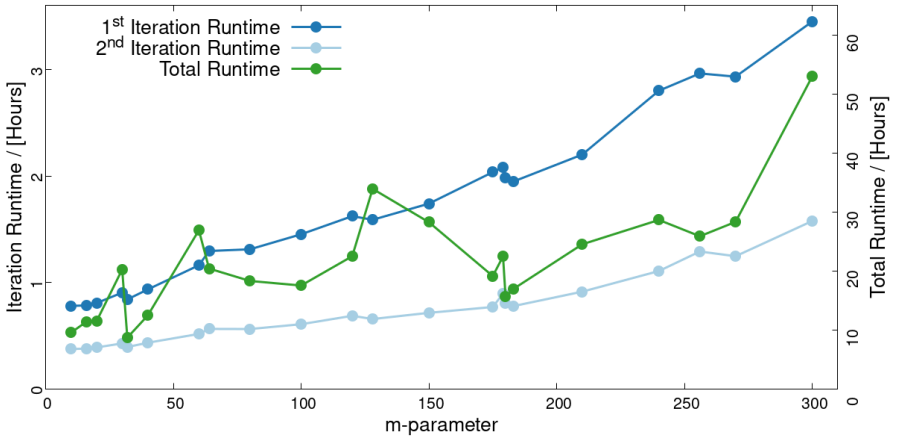

Figure 4.10: Runtimes, dependent on the m-parameter for the first and second optimization step of the DMRGSCF method. The runtime for the complete procedure is given on the secondary y-axis on the right. The time given is the real time as measured by the operating system.

As expected, the energy decreases with increasing m-parameter. There is, however, one exception at $m = 270$ where the energy of the electronic ground state did rise despite an increase of the m-parameter. We did not investigate the reason for this increase, but one possible

cause are local minima in which the algorithm might become trapped, and consequently fail to reach the global minimum for the given set of parameters.

This hypothesis is made plausible by the behavior for the runtime. While the time taken for the first and second iteration rises in a continuous fashion with the m-parameter, the total runtime has a far greater variability. This is indicative of highly variable convergence paths taken by the algorithm under variation of the m-parameter.

An analysis of total runtimes for the DMRGSCF algorithm in this manner was out of scope of the present work. Under the assumption that the preliminary (38, 30) and reduced (30, 26) active spaces are sufficiently similar, the data in Table 4.4 suggest that omitting the orbital optimization results in a variation of the excitation energies in the range of 0.2 eV for the present system. This variation is of the same magnitude as the one for variation of the ground state energy shown in Figure 4.9 during the increase of the the m-parameter from 256 to 300. It was thus determined to perform the dissociation analysis using an m-parameter of 250 and omit the orbital optimization step.

4.3 LIGAND DISSOCIATION

For dissociation analysis, the bond dissociation energy is the central quantity of interest. It is determined as the difference between the electronic ground state energy in the equilibrium geometry, and in a geometry where the ligands are at a distance large enough to be no longer considered as interacting electronically with the rest of the molecule.

4.3.1 *DFT Dissociation*

As a reference to improve on, electronic energies for the various fragments were calculated using DFT with the same parameters as for calculating the equilibrium geometry. Dissociation of a ligand was approximated by removing the atoms of the ligand under examination. This produced geometries for ligand and remainder fragments. The electronic energies for these fragments were then calculated separately. This yields the bond dissociation energy as the difference between the electronic energy at equilibrium and the sum of the electronic energies of the fragments:

$$E_{BD} = E_{GS} - \sum E_{Fragment} \tag{4.3.1}$$

The CO ligand in organometallic chemistry is counted as a neutral ligand and is a stable molecule by itself. Thus, the dissociated fragment was calculated as a neutral molecule. The NO fragment could, due to it's non-innocence as a ligand, conceivably dissociate while carrying a positive, neutral, or negative charge, leaving behind a residue with

Table 4.5: Bond dissociation energies for different fragments, calculated at the B3LYP/def2-TZVPP level of theory.

Dissociated Fragments	NO-Species	E_{BD} / eV
CO	-	2.203
NO	NO^+	12.70
	NO	3.678
	NO^-	12.72
NO + CO	NO^+	15.93
	NO	5.979
	NO^-	14.62

the corresponding neutralizing charge, thus all three possibilities were considered.

The results are given in Table 4.5. They suggest that the NO fragment would be unable to dissociate in a charged state by photodissociation under atmospheric conditions, as photon energies in excess of 10 eV require vacuum UV radiation [72]. The resulting dissociation energies for dissociation of uncharged NO are summarized in Figure 4.11.

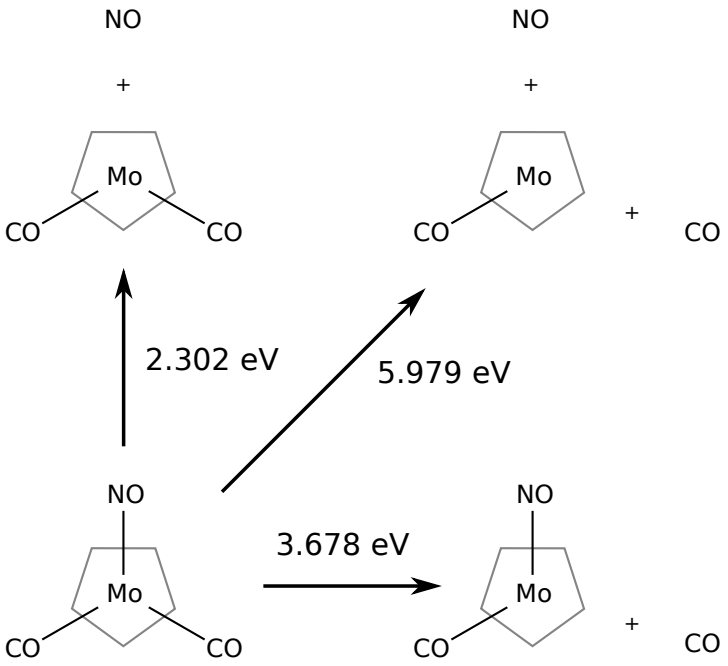

Figure 4.11: Bond dissociation energies.

4.3.2 *Bond Dissociation using DMRG*

Due to the runtime considerations in section 4.2.4 concerning the computational effort, the analysis of the ligand dissociation was performed without orbital optimization. To allow for flexibility in the molecular orbitals throughout the bond elongation, a step-wise procedure was devised:

The equilibrium geometry was chosen as a starting point. Hartree-Fock orbitals were generated and used as input for the DMRG-CI procedure, using the reduced active space described in Section 4.2.2. Then, the bonds under investigation were elongated to generate the next geometry along the bond dissociation coordinate. For this geometry, new Hartree-Fock orbitals were generated, using the orbitals of the previous DMRG-CI step as an initial guess. The resulting orbitals were compared to the guess orbitals. If necessary, orbitals were swapped so that the same orbitals remain in the active space. Then, the next DMRG-CI optimization step was performed. This procedure was repeated for each step along the dissociation coordinate.

For the dissociation of the NO-ligand, this approach proved to be difficult, as the Hartree-Fock method was prone to fail when the NO ligand was translated by a distance of more than 3 Å. The dissociation of NO was thus not further investigated in this work. For the dissociation of only the CO ligand, the electronic energies for the first eight electronic states are given in Figure 4.12, with a detail of the region close to the equilibrium geometry given in Figure 4.13.

The bond dissociation energy, given as the difference of the electronic energies of the ground state for a large separation of the ligand is in the range between 2.563 eV to 2.697 eV, as given in Table 4.6.

Table 4.6: Bond dissociation energy for CO as the energy difference between the electronic ground state at given distances.

Bond Elongation / Å	E_{BD} / eV
10	2.253
25	2.697
50	2.640

The variation of the ground state energy between the three investigated separation distances may be due to state averaging, which is used as an optimization criterion in the DMRG algorithm. Along the dissociation axis, the states may change their sensitivity to changes in the orbital coefficients. A more sensitive state may dominate the optimization procedure and drag the other states from their optimum. In particular, this may occur when adiabatic states undergo a change

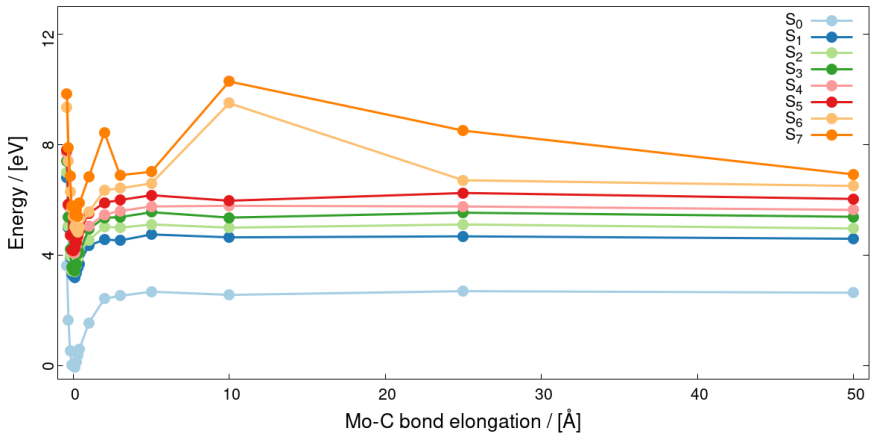

Figure 4.12: Energies calculated by DMRG-CI(30, 26)[250] of the electronic states, relative to the ground state energy at the equilibrium geometry under elongation of the Mo-CO bond distance.

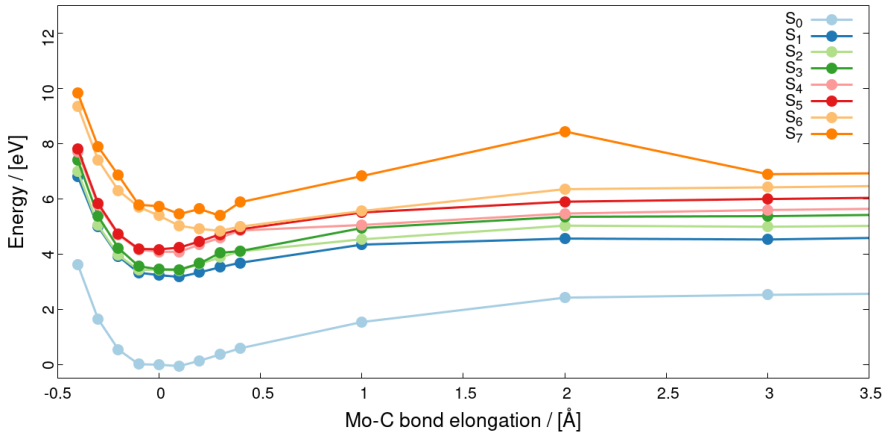

Figure 4.13: Energies calculated by DMRG-CI(30, 26)[250] of the electronic states, relative to the ground state energy at the equilibrium geometry under elongation of the Mo-CO bond distance. Detail of 4.12 showing the energies close to the equilibrium geometry.

of character. The increase in relative energy for the sixth and seventh excited state at an elongation of 10 Å is an indicator of such a change in character.

This effect of the state averaging, combined with the variational nature of the method, may also serve to explain the larger bond dissociation energy calculated by DMRG as compared to the DFT reference. At large separations, the selected active space which was optimized for the ground state may become less suitable if the characters of the electronic states change. This, in turn, necessarily leads to the calculation of a higher ground state energy compared to a calculation where the active space is also optimized for the dissociated geometries.

Thus, under the assumption that the choice of active space in equilibrium is reasonable, the bond dissociation energy would be overestimated by the DMRG method. By this argument, it is plausible that the bond dissociation energy of 2.253 eV, calculated at a bond elongation of 10 Å, is closer to both the value calculated using DFT and the true value.

5 CONCLUSION

The goal of this thesis was to investigate the photodissociation behavior of $CpMoNO(CO)_2$ and analyze the applicability of the DMRG method for this task. While a complete answer was outside the scope of this work, it was possible to gain some key insights that are useful for further analysis of the problem.

The structure of $CpMoNO(CO)_2$ is known through experimental means. Some minor uncertainty remains as to the assignment of the CO and NO ligands, which was decided with the aid of calculations [68]. In this work, the primary features of the structure, including the assignment of the ligands, could be reproduced using Density Functional Theory. The calculated structure was then used in the further analysis.

The excited electronic states were investigated for appreciable interaction with light in the visible range. The change in electronic density was used to identify states where the bond between the central ligand and one of the NO and CO ligands would be expected to weaken. These excited states are candidates for photodissociation of the molecule.

The molecule exhibits many traits that point to the necessity of a multiconfigurational approach, so the DMRG method was employed for this analysis. A suitable active space was sought to represent the excited electronic states identified in the previous step. Since no established protocol was available for this task, a selection protocol for single states [67] was extended to take into account excited states. The resulting active space was still considerably large. Therefore, benchmarks were created to tune the accuracy parameters of the method for further analysis steps.

Bond dissociation energies were calculated for the NO and CO ligands using both DFT and DMRG. For DFT, the system was separated into subsystems and for DMRG, the wave function was partially extended along a bond dissociation coordinate. The DMRG approach failed for the NO ligand, because wave functions at large ligand distances could not be obtained, and resolving this issue was outside the scope of this thesis. The dissociation energies, however, give a threshold for the energy required for photodissociation, and can be reached by experimental methods using optical lasers.

The main advantage of the DMRG method is that it allows the use of larger active spaces, compared to CI methods that do not truncate orbital interactions. It achieves this by limiting the number of possible interactions and selecting the most important contributions. In the

present thesis, it was shown that the orbital selection protocol was in alignment with chemical intuition in the identification of molecular orbitals with little contribution to the excited electronic states in question. Given an active space that encompasses the important orbitals, accuracy can then be balanced against the computational effort by tuning of a single parameter. The use of this parameter helps to decouple the selection of the active space from availability of computational resources.

The method still requires initial wave functions as a starting point for the optimization procedure. As encountered in this work, such wave functions may not be easily obtained for certain types of systems. However, this limitation is shared by other post-Hartree-Fock methods and not a singular feature of DMRG itself.

While the increased objectivity in the selection of active spaces is attractive for automation of quantum chemical analysis, a canonical ordering of molecular orbitals within the one-dimensional chain of subsystems seems to still be desirable. Orderings based on orbital entropies may require a way to be extended to multiple excited states, such as touched upon in this work with the extension of the selection protocol.

In conclusion, the method adds valuable tools to the repertoire of quantum chemistry, since it re-frames the restraints of active-space methods, and provides entanglement measures that contain information about the system, which is not only interpretable by chemical intuition but also enables comparisons between similar systems.

A

APPENDIX

A.1 GEOMETRY OPTIMIZATION

A.1.1 *Initial geometry optimization guess*

The initial geometry guess for the geometry optimization procedure is given in table A.1 as a Z-matrix [73].

A.1.2 *Equilibrium Geometry*

The optimized equilibrium geometry at the B3LYP/def-2-TZVPP level of theory, when using the Z-matrix in listing A.1 as a starting guess, is given in Table A.1 in cartesian coordinates, oriented so that the yz-plane coincides with the C_S mirror plane, and the z-axis is oriented closely to the C_5-axis of the Cp-ring.

Table A.1: Optimized equilibrium geometry, given in [Å].

Atom	x /[Å]	y /[Å]	z /[Å]
Mo	0.000	0.000	0.000
N	0.000	1.468	1.061
O	0.000	2.459	1.683
C	1.400	-0.883	1.114
O	2.232	-1.385	1.724
C	-1.400	-0.883	1.114
O	-2.232	-1.385	1.724
C	0.000	-1.328	-2.002
H	0.000	-2.404	-1.968
C	0.712	0.854	-2.141
H	1.345	1.723	-2.208
C	-0.712	0.854	-2.141
H	-1.345	1.723	-2.208
C	1.149	-0.489	-2.054
H	2.174	-0.820	-2.052
C	-1.149	-0.489	-2.054
H	-2.174	-0.820	-2.052

Listing A.1: Z-Matrix used as initial guess for geometry optimization of the staggered configuration.

```
xx
mo 1 moxx2
n 2 nmo3 1 nmoxx3
c 2 cmo4 1 cmoxx4 3 dih4 0
c 2 cmo4 1 cmoxx4 3 -dih4 0
o 3 on6 2 onmo6 5 dih6 0
o 4 oc7 2 ocmo7 5 dih7 0
o 5 oc7 2 ocmo7 4 dih7 0
c 1 cxx9 2 90. 3 dih9 0
c 1 cxx9 2 90. 3 dih10 0
c 1 cxx9 2 90. 3 -dih10 0
c 1 cxx9 2 90. 3 dih12 0
c 1 cxx9 2 90. 3 -dih12 0
h 9 hc14 2 hcmo14 3 180. 0
h 10 hc14 9 hcc14 14 dih15 0
h 11 hc14 9 hcc14 14 dih15 0
h 12 hc14 10 hcc14 15 dih15 0
h 13 hc14 11 hcc14 16 dih15 0

moxx2 2.
nmo3 1.8173
nmoxx3 120.
cmo4 1.99777
cmoxx4 120.
dih4 120.
on6 1.17004
onmo6 180.
dih6 120.
oc7 1.15177
ocmo7 180.
dih7 180.
cxx9 1.4
dih9 180.
dih10 253.
dih12 326.
hc14 1.08894
hcmo14 120.
dih15 0.
hcc14 120.
```

A.2 BOND ELONGATION INTERMEDIATE GEOMETRIES

The geometry inputs for bond elongation were calculated by taking the vectors $\vec{MoC}$ or $\vec{MoN}$ of the ground state geometry, creating a new vector $\vec{d}$ of the same direction and scaling it to the length of the bond elongation distance. This vector $\vec{d}$ was then added the coordinates of the atoms in the ligand under investigation to shift them along the bond axis to Mo. The bond elongation distances, given in Å, were: -0.4, -0.3, -0.2, -0.1, 0.1, 0.2, 0.3, 0.4, 1, 2, 3, 4, 10, 25, 50.

A.3 EXCITED STATES

The list of singlet excited states for the equilibrium geometry, calculated at the B3LYP/def2TZVPP level, is given in Table A.2, with the energy given in eV and the corresponding wavelength in nm.

A.4 MOLECULAR ORBITALS

This section gives the energies and iso-surfaces for the Hartree-Fock molecular orbitals generated with the the ANO-RCC-MB basis set at the optimized geometry. These orbitals were used for the DMRG configuration interaction.

Table A.3: List of molecular orbitals used in the DMRG-CASSCF-Procedure, calculated at the HF/ANO-RCC-MB level.

Orbital Number	Energy / $[E_h]$	Classification
1	-738.81	$1s(Mo)$
2	-107.25	$2s(Mo)$
3	-95.706	$2p(Mo)$
4	-95.705	$2p(Mo)$
5	-95.704	$2p(Mo)$
6	-20.777	$1s(O)$
7	-20.777	$1s(O)$
8	-20.690	$1s(O)$
9	-19.565	$3s(Mo)$
10	-15.808	$1s(N)$
11	-15.671	$3p(Mo)$
12	-15.668	$3p(Mo)$
13	-15.663	$3p(Mo)$
14	-11.553	$1s(C)$
15	-11.553	$1s(C)$
16	-11.367	$1s(Cp-C)$
17	-11.367	$1s(Cp-C)$
18	-11.366	$1s(Cp-C)$
19	-11.365	$1s(Cp-C)$
20	-11.355	$1s(Cp-C)$

Table A.3: List of molecular orbitals used in the DMRG-CASSCF-Procedure, calculated at the HF/ANO-RCC-MB level.

Orbital Number	Energy / $[E_h]$	Classification
21	-9.3123	$3d(Mo)$
22	-9.3118	$3d(Mo)$
23	-9.3071	$3d(Mo)$
24	-9.3014	$3d(Mo)$
25	-9.2982	$3d(Mo)$
26	-3.0599	$4s(Mo)$
27	-1.9326	$4p(Mo)$
28	-1.9148	$4p(Mo)$
29	-1.9110	$4p(Mo)$
30	-1.5863	$\sigma(NO)$
31	-1.5861	$\sigma'(CO)$
32	-1.5830	$\sigma(CO)$
33	-1.2678	$\sigma(Cp)$
34	-1.0439	$\sigma(Cp)$
35	-1.0399	$\sigma(Cp)$
36	-0.9724	$\sigma^*(NO)$
37	-0.8507	$\sigma^*(CO)$
38	-0.8392	$\sigma^{*\prime}(CO)$
39	-0.8053	$\sigma(Cp)$
40	-0.8043	$\sigma(Cp)$
41	-0.7782	$\sigma(Cp)$
42	-0.7207	$\pi(NO)$
43	-0.7133	$\sigma^*(CO), \sigma^*(NO)$
44	-0.7080	$\pi(CO), \sigma^*(NO)$
45	-0.7008	$\pi(NO, \pi(CO)$
46	-0.6987	$\pi(CO) - \sigma^*(NO)$
47	-0.6970	$\pi'(CO)$
48	-0.6904	$\pi_(CO) - \pi(NO)$
49	-0.6736	$\sigma^{*\prime}(CO)$
50	-0.6710	$\pi(CO) + \pi(NO)$
51	-0.6292	$\sigma^*(Cp)$
52	-0.6264	$\sigma^*(Cp)$
53	-0.6057	$\pi(Cp)$
54	-0.5993	$\sigma^*(Cp)$
55	-0.5977	$\sigma^*(Cp)$
56	-0.4299	$\pi_1(d(Mo) + \pi(Cp))$
57	-0.4255	$\pi_2(d(Mo) + \pi(Cp))$
58	-0.3671	$\pi_3(d(Mo) + \pi^*(NO) + \pi^*(CO))$
59	-0.3664	$\pi_4(d(Mo) + \pi^*(CO))$
60	-0.3639	$\pi_5(d(Mo) + \pi^*(CO))$
61	0.0356	$\pi_6(((d(Mo) + \pi^{*\prime}(CO)) + (d(Mo) - \pi^*(NO)))$
62	0.0510	$\pi^*(CO) + \pi^*(NO)$
63	0.0807	$\pi^{*\prime}(CO)$
64	0.1226	$\pi_1^*(d(Mo) - \pi^*(CO))$

Table A.3: List of molecular orbitals used in the DMRG-CASSCF-Procedure, calculated at the HF/ANO-RCC-MB level.

Orbital Number	Energy / $[E_h]$	Classification
65	0.1283	$\pi_2^*(d(Mo) - \pi^*(CO) - \pi^*(NO))$
66	0.1344	$\delta_1(d(Mo) + \pi^*(Cp), n(d(Mo), \pi^{*\prime}(CO))$
67	0.1813	$\pi_3^*(d(Mo) - \pi(Cp))$
68	0.1815	$\pi_4^*(d(Mo) - \pi(Cp)), n(d(Mo), \pi^{*\prime}(CO))$
69	0.2193	$\delta_1^*(d(Mo) - \pi^*(Cp))$
70	0.2303	$\delta_2^*(d(Mo) - \pi^*(Cp))$
71	0.2574	$5s(Mo)$
72	0.4343	
73	0.4456	
74	0.4531	
75	0.5113	
76	0.5125	
77	0.5213	
78	0.5286	
79	0.5384	
80	0.6053	
81	0.6096	
82	0.7384	
83	0.7788	
84	0.7989	
85	0.8167	
86	0.8995	
87	0.8999	

Table A.2: Electronic excited singlet states for the equilibrium geometry, calculated at the B3LYP/def2TZVPP level.

State	ΔE/[eV]	Wavelength/[nm]	Oscillator Strength
S_1	2.9057	426.70	0.011
S_2	2.9632	418.41	0.010
S_3	3.2700	379.16	0.000
S_4	3.4370	360.73	0.042
S_5	3.7095	334.24	0.008
S_6	4.1952	295.54	0.125
S_7	4.4923	275.99	0.148
S_8	4.6568	266.25	0.025
S_9	4.7186	262.75	0.002
S_{10}	4.8640	254.90	0.136
S_{11}	4.9230	251.85	0.095
S_{12}	5.0149	247.24	0.052
S_{13}	5.0311	246.43	0.092
S_{14}	5.1028	242.97	0.132
S_{15}	5.1494	240.77	0.022
S_{16}	5.1698	239.82	0.115
S_{17}	5.2300	237.07	0.008
S_{18}	5.3079	233.58	0.002
S_{19}	5.3869	230.16	0.036
S_{20}	5.4413	227.86	0.079
S_{21}	5.4801	226.25	0.254
S_{22}	5.5599	223.00	0.006
S_{23}	5.6079	221.09	0.066
S_{24}	5.6350	220.03	0.336
S_{25}	5.7824	214.42	0.306
S_{26}	5.8210	212.99	0.048
S_{27}	5.9313	209.04	0.070
S_{28}	6.0475	205.02	0.000
S_{29}	6.0695	204.27	0.664
S_{30}	6.0944	203.44	0.036

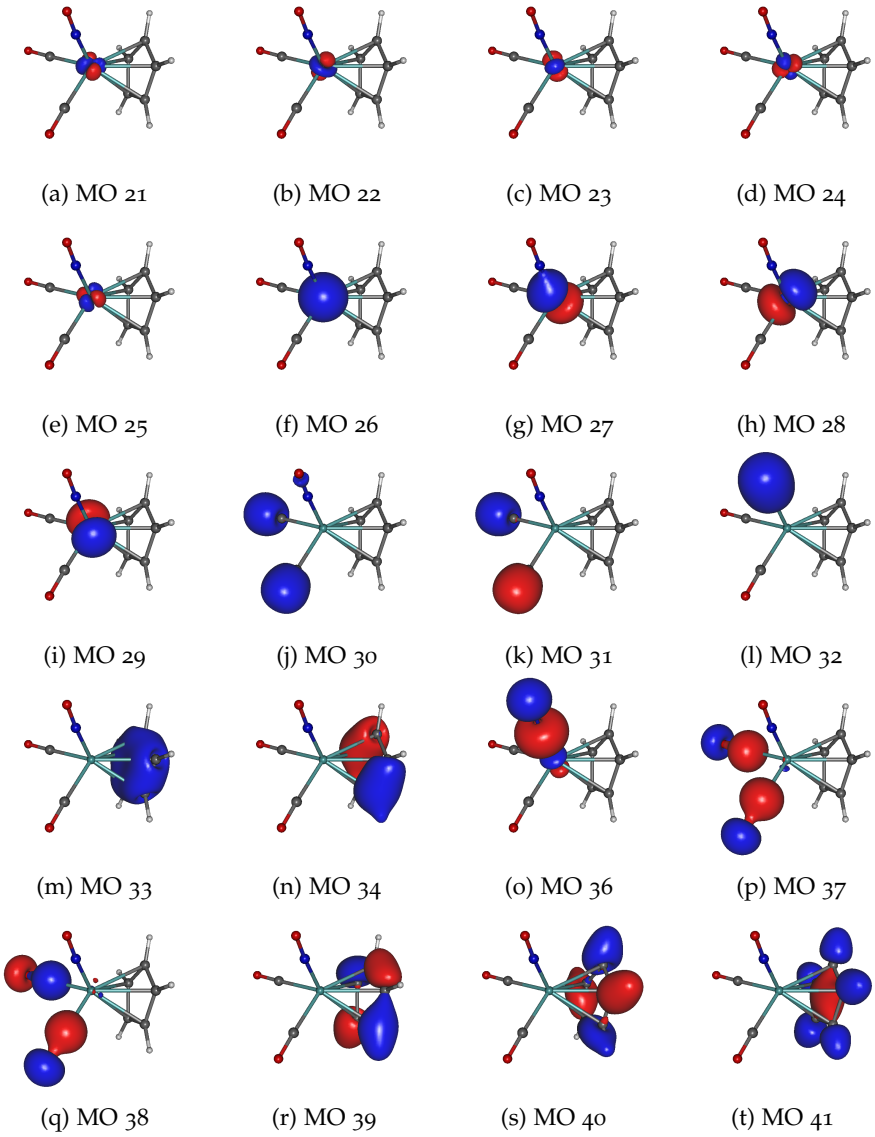

(a) MO 21 (b) MO 22 (c) MO 23 (d) MO 24

(e) MO 25 (f) MO 26 (g) MO 27 (h) MO 28

(i) MO 29 (j) MO 30 (k) MO 31 (l) MO 32

(m) MO 33 (n) MO 34 (o) MO 36 (p) MO 37

(q) MO 38 (r) MO 39 (s) MO 40 (t) MO 41

Figure A.1: Iso-surfaces of the molecular orbitals 21 to 41 for $|\psi| = 0.05$

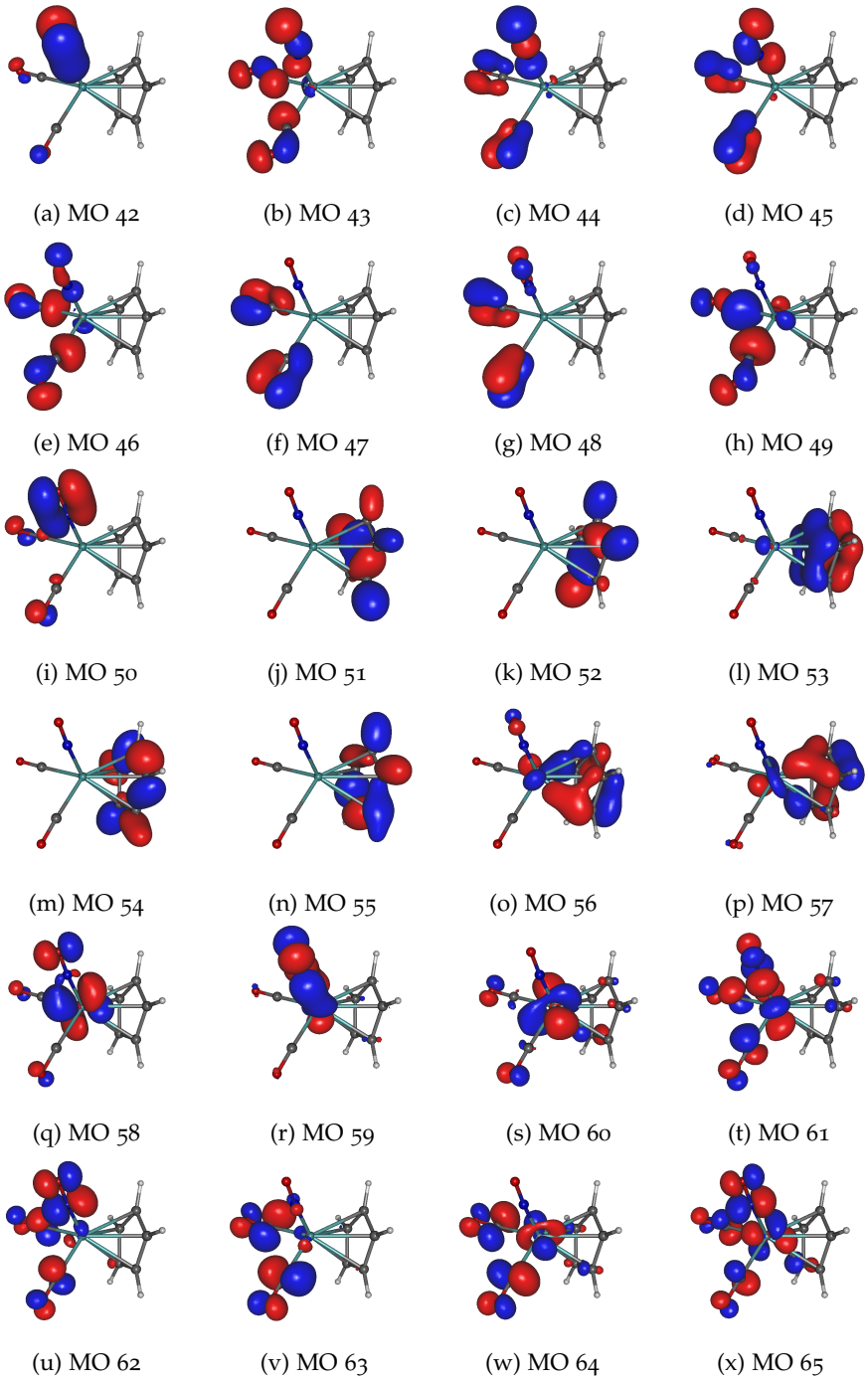

(a) MO 42 (b) MO 43 (c) MO 44 (d) MO 45

(e) MO 46 (f) MO 47 (g) MO 48 (h) MO 49

(i) MO 50 (j) MO 51 (k) MO 52 (l) MO 53

(m) MO 54 (n) MO 55 (o) MO 56 (p) MO 57

(q) MO 58 (r) MO 59 (s) MO 60 (t) MO 61

(u) MO 62 (v) MO 63 (w) MO 64 (x) MO 65

Figure A.2: Iso-surfaces of the molecular orbitals 42 to 65 for $|\psi| = 0.05$

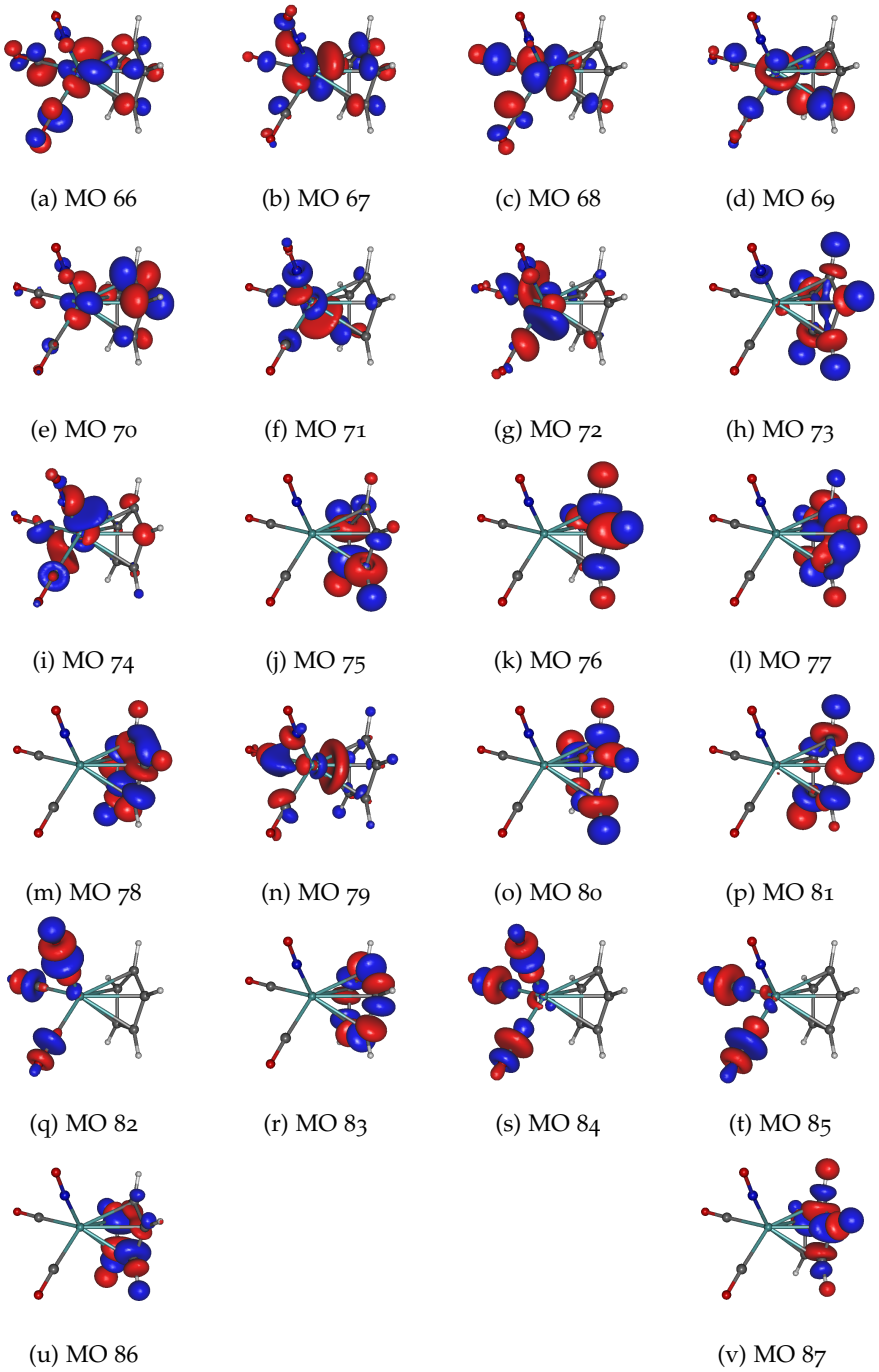

(a) MO 66 (b) MO 67 (c) MO 68 (d) MO 69

(e) MO 70 (f) MO 71 (g) MO 72 (h) MO 73

(i) MO 74 (j) MO 75 (k) MO 76 (l) MO 77

(m) MO 78 (n) MO 79 (o) MO 80 (p) MO 81

(q) MO 82 (r) MO 83 (s) MO 84 (t) MO 85

(u) MO 86 (v) MO 87

Figure A.3: Iso-surfaces of the molecular orbitals 66 to 87 for $|\psi| = 0.05$

A.5 DMRG RESULTS

A.5.1 *Single-Orbital Entanglement*

The Tables A.4 and A.5 give the values of the single-orbital entropies for the initial and the reduced active space, respectively.

Table A.4: Single-orbital entropies for the orbitals in the initial (30, 38) active space at different electronic states

Orbital	Electronic state							
	S0	S1	S2	S3	S4	S5	S6	S7
42	0.140	0.165	0.119	0.267	0.178	0.152	0.137	0.215
43	0.088	0.098	0.101	0.085	0.088	0.091	0.090	0.074
44	0.115	0.139	0.139	0.114	0.108	0.108	0.132	0.100
45	0.165	0.130	0.146	0.149	0.172	0.182	0.156	0.169
46	0.099	0.103	0.106	0.096	0.095	0.099	0.096	0.094
47	0.159	0.190	0.190	0.163	0.155	0.157	0.171	0.130
48	0.189	0.165	0.156	0.202	0.180	0.178	0.181	0.216
49	0.104	0.111	0.111	0.123	0.110	0.110	0.091	0.124
50	0.180	0.133	0.190	0.156	0.237	0.264	0.180	0.169
51	0.007	0.007	0.007	0.008	0.007	0.007	0.007	0.009
52	0.006	0.007	0.007	0.006	0.006	0.006	0.007	0.006
53	0.141	0.136	0.141	0.140	0.134	0.141	0.144	0.138
54	0.003	0.003	0.003	0.003	0.003	0.003	0.003	0.003
55	0.003	0.003	0.003	0.003	0.003	0.003	0.003	0.003
56	0.256	0.280	0.261	0.385	0.276	0.250	0.278	0.361
57	0.222	0.451	0.443	0.226	0.225	0.233	0.411	0.230
58	0.558	0.379	0.362	0.327	1.183	1.113	0.552	0.817
59	0.571	0.815	0.675	1.141	0.994	0.699	0.597	1.074
60	0.281	1.032	1.025	0.299	0.328	0.360	1.048	0.297
61	0.589	0.820	1.162	0.461	1.247	1.283	0.638	0.486
62	0.487	1.057	0.368	1.178	1.004	0.668	0.457	0.722
63	0.264	0.258	0.281	0.299	0.317	0.357	1.037	1.144
64	0.295	0.248	0.249	0.285	0.295	0.304	0.278	0.356
65	0.407	0.582	0.347	0.755	0.490	0.364	0.416	0.454
66	0.269	0.307	0.330	0.260	0.305	0.343	1.067	0.463
67	0.187	0.221	0.176	0.236	0.207	0.193	0.186	0.221
68	0.207	0.231	0.250	0.195	0.240	0.264	0.487	0.413
69	0.188	0.183	0.183	0.195	0.180	0.183	0.192	0.182
70	0.213	0.233	0.260	0.198	0.228	0.249	0.320	0.212
71	0.059	0.058	0.055	0.061	0.054	0.055	0.053	0.057

Table A.5: Single-orbital entropies for the orbitals in the reduced (26, 30) active space at different electronic states

Orbital	Electronic state							
	S0	S1	S2	S3	S4	S5	S6	S7
42	0.125	0.148	0.249	0.103	0.117	0.166	0.116	0.179
43	0.105	0.109	0.103	0.114	0.109	0.100	0.110	0.095
44	0.124	0.137	0.123	0.140	0.119	0.115	0.132	0.111
45	0.155	0.121	0.141	0.138	0.175	0.153	0.142	0.149
46	0.103	0.106	0.102	0.109	0.106	0.096	0.096	0.091
47	0.141	0.160	0.145	0.163	0.140	0.131	0.145	0.116
48	0.164	0.145	0.181	0.136	0.152	0.154	0.149	0.174
49	0.107	0.112	0.125	0.111	0.110	0.108	0.096	0.114
50	0.169	0.110	0.136	0.175	0.253	0.198	0.160	0.144
53	0.092	0.086	0.087	0.086	0.091	0.084	0.085	0.087
56	0.187	0.217	0.342	0.191	0.162	0.233	0.174	0.318
57	0.139	0.377	0.140	0.370	0.144	0.131	0.357	0.138
58	0.498	0.255	0.202	0.256	0.872	1.131	0.427	0.775
59	0.533	0.841	1.146	0.679	0.479	1.093	0.479	1.019
60	0.186	0.985	0.198	0.982	0.238	0.188	0.974	0.194
61	0.548	0.843	0.453	1.164	1.204	1.106	0.548	0.383
62	0.436	1.112	1.175	0.289	0.284	1.076	0.374	0.648
63	0.222	0.221	0.232	0.251	0.317	0.240	0.859	1.132
64	0.232	0.201	0.237	0.206	0.249	0.217	0.208	0.250
65	0.364	0.650	0.822	0.273	0.231	0.586	0.339	0.445
66	0.224	0.260	0.218	0.291	0.349	0.241	1.068	0.674
67	0.135	0.209	0.221	0.120	0.126	0.178	0.118	0.157
68	0.170	0.185	0.162	0.205	0.251	0.182	0.698	0.689
69	0.139	0.134	0.148	0.131	0.134	0.129	0.127	0.135
70	0.166	0.191	0.149	0.228	0.235	0.174	0.339	0.206
71	0.091	0.091	0.092	0.089	0.088	0.090	0.086	0.087

BIBLIOGRAPHY

[1] P. Agostinis et al. "Photodynamic therapy of cancer: An update." In: *CA: A Cancer Journal for Clinicians* 61.4 (2011), pp. 250–281.

[2] M. J. Paterson and L. T. Bergendahl. *Computational Modelling of the Steps Involved in Photodynamic Therapy*. IntechOpen, 2012. ISBN: 9789535104469.

[3] B. E. Mann. "CO-Releasing Molecules: A Personal View." In: *Organometallics* 31.16 (2012), pp. 5728–5735.

[4] N. L. Fry and P. K. Mascharak. "Photoactive Ruthenium Nitrosyls as NO Donors: How To Sensitize Them toward Visible Light." In: *Accounts of Chemical Research* 44.4 (2011). PMID: 21361269, pp. 289–298.

[5] B. Olas. "Carbon monoxide is not always a poison gas for human organism: Physiological and pharmacological features of CO." In: *Chemico-Biological Interactions* 222 (2014), pp. 37 –43. ISSN: 0009-2797.

[6] D. M. Evans. *Nitric oxide: Emerging developments, therapeutic role in disease states and health effects*. English. Nova Science Publishers, Inc., 2015. ISBN: 9781634830164.

[7] P. Ledgzdins, C. C. Y. Pang, and M. J. Shaw. *United States Patent 5,631,284 - Compositions and methods for relaxing smooth muscles*. May 1997.

[8] R. Mendel and S. Leimkühler. "The biosynthesis of the molybdenum cofactors." eng. In: *JBIC Journal of Biological Inorganic Chemistry* 20.2 (2015), pp. 337–347. ISSN: 0949-8257.

[9] A. Vyskocil. "Assessment of molybdenum toxicity in humans." In: *Journal of applied toxicology.* 19.3 (1999), pp. 185–192. ISSN: 0260-437X.

[10] G. A. Leichtmann. "Update on trace elements." In: *Comprehensive Therapy* 17.1 (1991), pp. 42–48. ISSN: 0098-8243.

[11] *Toxicology and carcinogenesis studies of molybdenum trioxide in F344/N rats and B6C3F1 mice (inhalation studies). Technical Report Series No. 462, NIH Publication No. 97-3378, PMID: 12587014*.

[12] C. J. Cramer and D. G. Truhlar. "Density functional theory for transition metals and transition metal chemistry." In: *Phys. Chem. Chem. Phys.* 11 (46 2009), pp. 10757–10816.

[13] C. K. Jørgensen. "Differences between the four halide ligands, and discussion remarks on trigonal-bipyramidal complexes, on oxidation states, and on diagonal elements of one-electron energy." In: *Coordination Chemistry Reviews* 1.1 (1966), pp. 164 –178. ISSN: 0010-8545.

[14] W. Kaim and B. Schwederski. "Non-innocent ligands in bioinorganic chemistry - An overview." In: *Coordination Chemistry Reviews* 254.13 (2010). Dithiolenes and non-innocent redox-active ligands, pp. 1580 –1588. ISSN: 0010-8545.

[15] W. E. Geiger, P. H. Rieger, B. Tulyathan, and M. D. Rausch. "Evidence for bending of a nitrosyl group during one-electron reduction of cyclopentadienyl metal nitrosyl compounds." In: *Journal of the American Chemical Society* 106.23 (1984), pp. 7000–7006. ISSN: 0002-7863.

[16] L. Freitag, S. Knecht, S. F. Keller, M. G. Delcey, F. Aquilante, T. B. Pedersen, R. Lindh, M. Reiher, and L. González. "Orbital entanglement and CASSCF analysis of the Ru–NO bond in a Ruthenium nitrosyl complex." In: *Phys. Chem. Chem. Phys.* 17 (22 2015), pp. 14383–14392.

[17] K. H. Marti and M. Reiher. "The Density Matrix Renormalization Group Algorithm in Quantum Chemistry." In: *Zeitschrift für Physikalische Chemie* 224.3-4 (2010), pp. 583 –599.

[18] G. K.-L. Chan and S. Sharma. "The Density Matrix Renormalization Group in Quantum Chemistry." In: *Annual Review of Physical Chemistry* 62.1 (2011). PMID: 21219144, pp. 465–481.

[19] Y. Kurashige. "Multireference electron correlation methods with density matrix renormalisation group reference functions." In: *Molecular Physics* 112.11 (2014), pp. 1485–1494.

[20] S. Wouters and D. Van Neck. "The density matrix renormalization group for ab initio quantum chemistry." In: *The European Physical Journal D* 68.9 (2014), p. 272.

[21] T. Yanai, Y. Kurashige, W. Mizukami, J. Chalupský, T. N. Lan, and M. Saitow. "Density matrix renormalization group for ab initio Calculations and associated dynamic correlation methods: A review of theory and applications." In: *International Journal of Quantum Chemistry* 115.5 (2015), pp. 283–299.

[22] S. Sharma and G. K.-L. Chan. "Spin-adapted density matrix renormalization group algorithms for quantum chemistry." In: *The Journal of Chemical Physics* 136.12 (2012), p. 124121.

[23] L. Freitag, L. Lindenbauer, M. Oppel, and L. González. "A Density Matrix Renormalization Group Study of the Low-Lying Excited States of a Molybdenum Carbonyl-Nitrosyl Complex." In: *ChemPhysChem* 22.22 (), pp. 2371–2377. ISSN: 1439-4235, 1439-7641.

[24] E. Schrödinger. "An Undulatory Theory of the Mechanics of Atoms and Molecules." In: *Physical Review* 28.6 (Dec. 1, 1926), pp. 1049–1070. ISSN: 0031-899X.

[25] E. Schrödinger. "Quantisierung als Eigenwertproblem." In: *Annalen der Physik* 384.4 (1926), pp. 361–376. ISSN: 00033804, 15213889.

[26] F. Jensen. *Introduction to computational chemistry*. eng. Third edition. Chichester: Wiley, 2017. ISBN: 9781118825990.

[27] P. A. M. Dirac. "A new notation for quantum mechanics." In: *Mathematical Proceedings of the Cambridge Philosophical Society* 35.3 (July 1939), pp. 416–418. ISSN: 0305-0041, 1469-8064.

[28] M. Born and R. Oppenheimer. "Zur Quantentheorie der Molekeln." In: *Annalen der Physik* 389.20 (1927), pp. 457–484. ISSN: 00033804, 15213889.

[29] D. R. Hartree. "The Wave Mechanics of an Atom with a Non-Coulomb Central Field. Part I. Theory and Methods." In: *Mathematical Proceedings of the Cambridge Philosophical Society* 24.1 (Jan. 1928), pp. 89–110. ISSN: 0305-0041, 1469-8064.

[30] P. W. Atkins. *Quanten: Begriffe und Konzepte für Chemiker*. ger. Weinheim [u.a.]: VCH-Verl.-Ges., 1993. ISBN: 3527290826.

[31] J. C. Slater. "The Theory of Complex Spectra." In: *Physical Review* 34.10 (Nov. 15, 1929), pp. 1293–1322. ISSN: 0031-899X.

[32] A. Szabo and N. Ostlund. *Modern Quantum Chemistry: Introduction to advanced electronic structure theory*. eng. 1. ed., rev. Mineola, NY: Dover Publ., 1996. ISBN: 9780486691862.

[33] C. C. J. Roothaan. "New Developments in Molecular Orbital Theory." In: *Reviews of Modern Physics* 23.2 (Apr. 1, 1951), pp. 69–89. ISSN: 0034-6861.

[34] J. E. Avery and J. S. Avery. "Molecular integrals for slater type orbitals using coulomb sturmians." In: *Journal of Mathematical Chemistry* 52.1 (Jan. 2014), pp. 301–312. ISSN: 1572-8897.

[35] F. E. Harris and H. H. Michels. "The Evaluation of Molecular Integrals for Slater-Type Orbitals." In: *Advances in Chemical Physics*. John Wiley & Sons, Ltd, 2007, pp. 205–266. ISBN: 9780470140154.

[36] S. F. Boys. "Electronic wave functions - I. A general method of calculation for the stationary states of any molecular system." In: *Proceedings of the Royal Society of London. Series A.* 200.1063 (Feb. 22, 1950), pp. 542–554. ISSN: 2053-9169.

[37] T. Petersson and B. Hellsing. "Adetailed derivation of gaussian orbital-based matrix elements in electron structure calculations." eng. In: *European Journal of Physics* 31.1 (2010), pp. 37–46. ISSN: 0143-0807.

[38] M. Hô and J.-M. Hernández-Pérez. "Evaluation of Gaussian Molecular Integrals." In: *The Mathematica Journal* 14 (2012). ISSN: The Mathematica Journal.

[39] W. Koch. *A chemist's guide to density functional theory*. eng. 2. ed.. Weinheim [u.a.]: WILEY-VCH, 2001. ISBN: 9783527304226.

[40] C. Ullrich. *Time-dependent density-functional theory: concepts and applications*. eng. Oxford graduate texts. Oxford : Oxford University Press, 2012. ISBN: 0-19-884193-0.

[41] P. Hohenberg and W. Kohn. "Inhomogeneous Electron Gas." In: *Physical Review* 136.3 (Nov. 9, 1964), B864–B871. ISSN: 0031-899X.

[42] W. Kohn and L. J. Sham. "Self-Consistent Equations Including Exchange and Correlation Effects." In: *Physical Review* 140.4 (Nov. 15, 1965), A1133–A1138. ISSN: 0031-899X.

[43] E. Runge and E. K. U. Gross. "Density-Functional Theory for Time-Dependent Systems." In: *Phys. Rev. Lett.* 52 (12 1984), pp. 997–1000.

[44] C. J. Cramer. *Essentials of computational chemistry: theories and models*. eng. Reprint.. Chichester [u.a.]: Wiley, 2004. ISBN: 0471485519.

[45] D. C. Young. *Computational chemistry: a practical guide for applying techniques to real world problems*. eng. New York: Wiley, 2001. ISBN: 0471458430.

[46] T. Helgaker, P. Jørgensen, and J. Olsen. *Molecular electronic-structure theory*. eng. Chichester; New York: Wiley, 2000. ISBN: 9781119019565.

[47] S. R. White. "Density matrix formulation for quantum renormalization groups." In: *Phys. Rev. Lett.* 69 (19 1992), pp. 2863–2866.

[48] G. K.-L. Chan and S. Sharma. "The Density Matrix Renormalization Group in Quantum Chemistry." In: *Annual Review of Physical Chemistry* 62.1 (2011), pp. 465–481.

[49] K. H. Marti and M. Reiher. "New electron correlation theories for transition metal chemistry." In: *Physical Chemistry Chemical Physics* 13.15 (2011), p. 6750. ISSN: 1463-9076, 1463-9084.

[50] L. Freitag. "Quantum chemical studies on electronic structure and photodynamics of ruthenium complexes." PhD thesis. Vienna: University of Vienna, 2015.

[51] J. Rissler, R. M. Noack, and S. R. White. "Measuring orbital interaction using quantum information theory." In: *Chemical Physics* 323.2-3 (Apr. 2006), pp. 519–531. ISSN: 0301-0104.

[52] U. Schollwöck. "The density-matrix renormalization group." English. In: *Reviews Of Modern Physics* 77.1 (2005), pp. 259–315. ISSN: 0034-6861.

[53] S. Keller, M. Dolfi, M. Troyer, and M. Reiher. "An efficient matrix product operator representation of the quantum chemical Hamiltonian." In: *The Journal of Chemical Physics* 143.24 (2015), p. 244118.

[54] M. J. Frisch et al. *Gaussian 16 Revision C.01*. Gaussian Inc. Wallingford CT. 2016.

[55] A. D. Becke. "Density-functional thermochemistry. III: The role of exact exchange." In: *The Journal of Chemical Physics* 98.7 (1993), pp. 5648–5652. ISSN: 00219606.

[56] F. Weigend and R. Ahlrichs. "Balanced basis sets of split valence, triple zeta valence and quadruple zeta valence quality for H to Rn: Design and assessment of accuracy." In: *Physical Chemistry Chemical Physics* 7.18 (2005), pp. 3297–3305. ISSN: 1463-9076.

[57] B. O. Roos, R. Lindh, P.-Å. Malmqvist, V. Veryazov, and P.-O. Widmark. "New Relativistic ANO Basis Sets for Transition Metal Atoms." In: *The Journal of Physical Chemistry A* 109.29 (2005). PMID: 16834004, pp. 6575–6579.

[58] M. Reiher. "Relativistic Douglas–Kroll–Hess theory." eng. In: *Wiley Interdisciplinary Reviews: Computational Molecular Science* 2.1 (2012), pp. 139–149. ISSN: 1759-0876.

[59] S. Keller, M. Dolfi, M. Troyer, and M. Reiher. "An efficient matrix product operator representation of the quantum chemical Hamiltonian." In: *The Journal of Chemical Physics* 143.24 (2015), p. 244118.

[60] L. Freitag, S. Keller, S. Knecht, R. Lindh, Y. Ma, C. J. Stein, and M. Reiher. *In preparation*. URL: reiher.ethz.ch/software/maquis.html (visited on 04/17/2023).

[61] I. F. Galván et al. "OpenMolcas: From Source Code to Insight." In: *Journal of Chemical Theory and Computation* 15.11 (2019). PMID: 31509407, pp. 5925–5964.

[62] F. Plasser. *TheoDORE: a package for theoretical density, orbital relaxation, exciton analysis, available from http://theodore-qc.sourceforge.net/.*

[63] C. J. Stein and M. Reiher. "Automated Selection of Active Orbital Spaces." In: *Journal of Chemical Theory and Computation* 12.4 (2016). PMID: 26959891, pp. 1760–1771.

[64] C. J. Stein, V. von Burg, and M. Reiher. "The Delicate Balance of Static and Dynamic Electron Correlation." In: *Journal of Chemical Theory and Computation* 12.8 (2016). PMID: 27409981, pp. 3764–3773.

[65] C. J. Stein and M. Reiher. "Measuring multi-configurational character by orbital entanglement." In: *Molecular Physics* 115.17-18 (2017), pp. 2110–2119.

[66] C. J. Stein and M. Reiher. "Automated Identification of Relevant Frontier Orbitals for Chemical Compounds and Processes." In: *CHIMIA International Journal for Chemistry* 71.4 (2017), pp. 170–176. ISSN: 0009-4293.

[67] C. J. Stein and M. Reiher. "Automated Selection of Active Orbital Spaces." In: *Journal of Chemical Theory and Computation* 12.4 (Mar. 2016), pp. 1760–1771. ISSN: 1549-9626.

[68] M. Schwalbe, P. C. Andrikopoulos, D. R. Armstrong, J. Reglinski, and M. D. Spicer. "Structural and Theoretical Insights into Metal–Scorpionate Ligand Complexes." In: *European Journal of Inorganic Chemistry* 2007.10 (2007), pp. 1351–1360.

[69] D. J. Parker and M. H. B. Stiddard. "Vibrational and electronic spectra of transition-metal carbonyl complexes. Part VII: Infrared spectra of some cyclopentadienyl-metal carbonyl complexes." In: *J. Chem. Soc. A* (1970), pp. 480–490.

[70] R. D. Johnson III, ed. *NIST Computational Chemistry Comparison and Benchmark Database. NIST Standard Reference Database Number 101*. Version Release 20. Aug. 2019. URL: http://cccbdb.nist.gov/.

[71] G. O. Spessard and G. Miessler. *Organometallic chemistry*. eng. Third edition. New York, Oxford [u.a.]: Oxford University Press, 2016. ISBN: 9780199342679.

[72] *ISO 21348: Definitions of Solar Irradiance Spectral Categories*. Standard. International Organization for Standardization.

[73] D. C. Young. *Computational chemistry: a practical guide for applying techniques to real world problems*. eng. New York: Wiley, 2001. ISBN: 0471458430.